

PAPER

Passive piezoelectric subordinate oscillator arrays

To cite this article: Sai Tej Paruchuri *et al* 2019 *Smart Mater. Struct.* **28** 085046

View the [article online](#) for updates and enhancements.

You may also like

- [Cascaded semiconductor optical amplifiers-based all-optical OR logic gate](#)
Amer Kotb, Kyriakos E Zoiros and Wei Li

- [Least-squares \(LS\) deconvolution of a series of overlapping cortical auditory evoked potentials: a simulation and experimental study](#)
Fabrice Bardy, Bram Van Dun, Harvey Dillon et al.

- [Theory of four-wave mixing in quantum dot semiconductor optical amplifiers](#)
Ahmed H Flayyih and Amin H Al-Khursan



The Electrochemical Society
Advancing solid state & electrochemical science & technology

243rd ECS Meeting with SOFC-XVIII


More than 50 symposia are available!

Present your research and accelerate science

Boston, MA • May 28 – June 2, 2023

[Learn more and submit!](#)

Passive piezoelectric subordinate oscillator arrays

Sai Tej Paruchuri^{1,4} , John Sterling², Vijaya V N Sriram Malladi¹, Andrew Kurdila¹, Joseph Vignola³ and Pablo Tarazaga¹

¹Department of Mechanical Engineering, Virginia Tech, Blacksburg, VA, United States of America

²Naval Surface Warfare Center, Carderock Division, Bethesda, MD, United States of America

³School of Engineering, The Catholic University of America, Washington, DC, United States of America

E-mail: saitejp@vt.edu, john.a.sterling1@navy.mil, sriram@vt.edu, kurdila@vt.edu, vignola@cua.edu and ptarazag@vt.edu

Received 12 April 2019

Accepted for publication 4 July 2019

Published 25 July 2019



CrossMark

Abstract

Subordinate oscillator arrays (SOAs) attached to a host structure have been shown to achieve flat attenuation of the frequency response over a band around a target natural frequency of the host. Due to their sensitivity to disorders that can arise from sources such as fabrication errors, as well as uncertainties in their structural properties or that of the host, SOAs can be challenging to implement in some applications. To overcome this shortcoming, piezoelectric subordinate oscillator arrays (PSOAs) are studied in this paper. This paper models PSOAs using variational principles to facilitate the analysis and development of design strategies. A closed-form expression for the frequency response function of the host structure is then used to design the PSOAs with and without uncertainties. This paper shows that the flat attenuation over a frequency band around a harmonic of the host can be achieved by assigning a distribution to the mechanical, electrical, or electromechanical properties of the PSOAs. For instance, it is shown that choosing a distribution of capacitive shunt circuits can achieve essentially the same qualitatively flat attenuation as that of classical SOAs. In this sense, the approach in this paper generalizes the results attained for conventional SOAs. Finally, the paper investigates the robustness of PSOAs, that is, their relative insensitivity to types of uncertainties. It is shown that PSOAs afford the chance to ameliorate some types of sensitivities that prove problematic for SOAs that are purely mechanical in nature. The notion of *performance recovery* is introduced; this measure quantifies how much attenuation loss due to uncertainty in an initial SOA or PSOA design can be recovered by modification of the electrical properties alone.

Keywords: piezoelectric subordinate oscillator arrays, shunt tuning, performance recovery, broadband flat vibration attenuation

(Some figures may appear in colour only in the online journal)

1. Introduction

The vibrations community has studied vibration attenuation of a host structure of given structural properties using attached substructures for decades. One classic example is a dynamic vibration absorber (DVA) attached to a host structure, which now appears as a typical example in vibration textbooks [1]. By analyzing the frequency response function, one can conclude that a DVA is a simple yet effective method

for vibration attenuation. However, DVAs achieve attenuation only in a narrow frequency band around a particular frequency of operation. Any variation in the driving frequency can render the DVA ineffective, and it is known that the response is amplified at some nearby, off-resonance driving frequencies. Thus, if the driving frequency changes, a classical DVA has to be re-tuned, that is it must be re-built, to match the new input frequency.

It is well-known that these potential disadvantages of a classical DVA have been addressed in many ways. To achieve a broader frequency range of vibration reduction, damped

⁴ Author to whom any correspondence should be addressed.

vibration absorbers have been used. Many investigators have proposed methods which optimize parameters of damped vibration absorbers [2–6]. Researchers have tried to overcome these limitations by attaching the host structure to an array of linear vibration absorbers whose natural frequencies form a band in the frequency domain [7–11]. This is possible when the frequency band of the array is spaced around the host structure's natural frequency. These arrays of oscillators have been referred to in the literature as Subordinate Oscillator Arrays, or SOAs. At first, designing an SOA might look like a complicated task since designers are forced to choose the structural properties of multiple absorbers. Vignola *et al* [11] show that simple 'closed form' design strategies, ones that do not require optimization, that prescribe distributions representing the structural properties of the SOA makes implementing SOAs much more straightforward in practice.

At the same time, a large number of piezoelectric systems have been studied to achieve a variety of engineering goals. Some of the most recent are summarized in table 1. In section 2 we review these references in more detail, but here we note that many of these references seek to develop passive and active vibration absorbers. Other papers in the table obtain vibration attenuation as a byproduct of their research: methods for energy harvesting from structures naturally induce attenuation of structural response.

Perhaps surprisingly, there is little or no formal overlap between the study of mechanical domain SOAs and the literature on composite piezoelectric systems to achieve vibration attenuation. In particular, none of the references in table 1 discuss, or even refer to, the notion of introducing distributions or mixtures of properties (as in [7–11]) of attached piezoelectric arrays connected to a host. In view of this fact, one of the overall and guiding aims of this paper is to explore how the philosophy of design for SOAs in [11] in terms of distributions of properties can be extended to arrays of piezoelectric SOAs or PSOAs.

The answer to this general question is that assigning distributions of electromechanical properties of PSOAs defines a theoretically sound, closed form, simple, effective strategy to achieve vibration attenuation in a host structure. From a technical standpoint, the efficacy of the method can be traced to finding a closed form expression for the frequency response function from input excitation to the host response. In this expression, which is valid for an arbitrary number of attached piezoelectric elements, all the electromechanical degrees of freedom of the PSOA have been eliminated. It is the specific zero-nonzero block structure of the coupled equations governing the PSOA and the (non-piezoelectric) host (see equations (12) below) that allow the elimination of all piezoelectric states.

To be sure, the governing equations for a PSOA coupled to a host are indeed a very special type of linear piezoelectric system, and such a simple reduction cannot be carried out in general linearly elastic piezoelectric systems. Note that this zero-nonzero block structure does not, in general, arise for instance in modal or finite element approximations of 'monolithic' linear, distributed piezoelectric continua models such as used for beams, plates, or shells, such as those modeled in a general form in [12], or in many of the references in table 1. It is conceivable that such a

block structure, and subsequent elimination of the piezoelectric states, could be carried out with the introduction of static or Guyan reduction, the definition of independent and dependent coordinates or other component mode synthesis approaches [13]. See the comments following equation (13). However, this process amounts to another level of approximations beyond and in addition to discretization, one that is nontrivial and sometimes impossible to carry out. In any event, it is the specific block structure of the PSOA and host equations that enables the closed form expression for the FRF of the host to be derived.

In the remainder of this paper, we begin with a careful literature review of related electromechanical modeling of piezoelectric systems in section 2. Section 3 summarizes the relevant technical background for SOAs. Section 4 describes models for PSOAs, while section 5 summarizes the derivation of the frequency response function from the input to the host response when it is equipped with a PSOA. The closed form design strategies, including the specific discussion of mass distribution-only and capacitance-distribution-only methods, is given in section 5. The experimental setup is introduced in section 6, section 7 summarizes the numerical simulations of the experiment, and 8 reviews the experimental results. The conclusions of the paper are given in section 9.

2. Piezoelectric structures literature review

Researchers have studied active and passive structures based on piezoelectric materials for vibration attenuation for some time, and an extensive literature on this topic has accumulated over the years. The term piezoelectric system covers a wide range of nuanced systems that vibration engineers and researchers have used for a variety of applications. Just within the field of vibration attenuation, we can classify piezoelectric systems into multiple categories based on the methodology used to achieve attenuation. The objective of this section is to highlight the similarities and the differences of such systems described in the literature with the one discussed in this paper.

Indeed, one glaring difference between many studies of composite piezoelectric systems and that tackled in this paper is that the latter system is made up of a family of linear oscillators that are connected to the host structure. That is, the piezoelectric components are only connected to the host, not to each other. Even though the oscillators in the PSOA are not coupled to each other, the coupling arises through the host. Thus, the response of the PSOA in itself is not of particular interest in this context, and the primary focus of this paper is on the input-output response of the host structure coupled with a PSOA. This fact stands in stark contrast to many models of distributed active piezoelectric systems that are studied in the literature. Furthermore, as mentioned above, the nature of the PSOA connection to the host creates a coupled linear ODE that enables the derivation of a closed-form expression for host frequency response function. This expression makes it easier to develop well-defined design techniques with predictable performance.

Further, some of the topics that are not traditionally discussed on papers on linear piezoelectric systems, but are addressed here, include: (1) the effect of robustness and

Table 1. Relevant piezoelectric systems literature summary.

General type	Reference(s)
SOAs	[10] 2012, [11] 2009, [15] 2012, [16] 2016, [8] 2005, [7] 1996, [17] 2001, [18] 1997, [9] 2005
Qualitative, numerical, and experimental study of piezoelectric systems with shunt circuits	[19] 1990, [20] 2000, [21] 2000, [22] 2001, [23] 2001, [24] 2006, [25] 2010, [26] 2011, [27] 2011, [26] 2011, [28] 2011, [29] 2011, [30] 2012, [31] 2012, [32] 2012, [31] 2012, [32] 2012, [33] 2013, [34] 2014, [35] 2014, [36] 2016, [37] 2016, [38] 2017
Mechanical SDOF or MDOF system, state switched or semi-active piezoelectric DVAs	[39] 1999, [40] 1999, [41] 2000, [42] 2000, [43] 2001, [44] 2001, [45] 2002, [46] 2004, [47] 2006, [48] 2006, [49] 2008, [50] 2009, [51] 2010, [52] 2011, [53] 2012
Gain scheduled or operating mode switched piezoelectric composite DVAs	[54] 1997, [55] 1998, [56] 2000
Optimization-based DVA analysis and design	[57] 2003, [58] 2012, [59] 2014
Piezoelectric energy harvesting, unswitched or switched	[54] 1997, [55] 1998, [56] 2000, [60] 2010, [61] 2009, [62] 2007, [63] 2013, [64] 2006, [65] 2005, [66] 2009, [67] 2012, [68] 2012, [69] 2012, [70] 2003
Metamaterials and wave propagation design and tailoring	[71] 2011, [72, 73] 2013, [74] 2013, [75] 2015, [76] 2016, [77] 2016, [78] 2017, [79] 2017, [80] 2017, [81] 2017

uncertainty on the performance of a design; (2) the development of a simple general design approach that relies on the distributions of electromechanical properties of the PSOA; and (3) an analysis of the performance recovery ability of a PSOA.

Because of the sheer number of studies of piezoelectric systems for vibrations attenuation, the only the most relevant categories of research are reviewed here. Table 1 shows each general category and a corresponding list of papers that fall under a category. Of course, some of these studies can fall under multiple categories. Such studies have been classified based on the authors' assessment of the principal features of the approach. Piezoelectric systems have been studied for more than half a century, and one of the earliest references is [14]. However, most of the papers presented in table 1 are from studies conducted in the past 25 years. In addition to the piezoelectric systems shown in table 1, SOAs have been included as a category due to its similarity to the system presented in this paper. PSOAs can be seen as a generalization of SOAs or as a particular case of coupled linearly piezoelectric systems. Discussions on these systems appear regularly in this paper since these systems have inspired PSOAs.

The largest category in table 1 is the one that contains piezoelectric equivalents of DVAs. The papers in the category include qualitative, numerical and experimental studies of piezoelectric oscillators with shunt circuits. In the studies, the mechanical part of the systems has been modeled using lumped (both single degree of freedom and multi-degree of freedom) as well as distributed parameter systems. The associated shunt circuits have been modeled as passive (using RLC circuits) and active systems. When passive electrical circuits are attached, these can be understood either as attempts to change the effective properties of the whole system or to induce

(additional) poles and harmonics into the system response of the original structure. The papers in this category have discussed the modeling and design of piezoelectric systems. While these systems provide a theoretical framework for the design and analysis of PSOAs, they do not exploit the specific structural advantages of the PSOA and host system. Further, these papers do not discuss the robustness of the systems and performance recovery using shunt tuning. In essence, the PSOA systems can be thought of as a combination of SOAs and the piezoelectric systems in this category.

The third category in table 1 includes the systems that use state switching to achieve parameter shifts in electromechanical properties of a structure. For example, it is well-known that by switching between two capacitances, one can change the effective stiffness and hence the natural frequency of the system. These systems are sometimes considered as semi-active systems since these systems switch between passive circuits, at the expense of the relatively low energy consumed to power the switches, in contrast to modulating voltage or current in the shunt circuit. Several studies in table 1 investigating this effect can be found in the past two decades. However, a general study of robustness of these systems has not been undertaken in these references. We will argue that the use of flat-band solutions like PSOAs can be an effective alternative to some of these systems, especially when the frequency band of operation is known and restricted to a fewer number of resonant peaks. This is demonstrated in particular in the conclusions in section 9.

Another recent class of systems which have attracted the interest of the vibrations community are those that are associated with metamaterials and waveguide design. Metamaterials are composed of an identical array of substructures that are periodically distributed along the length of the host

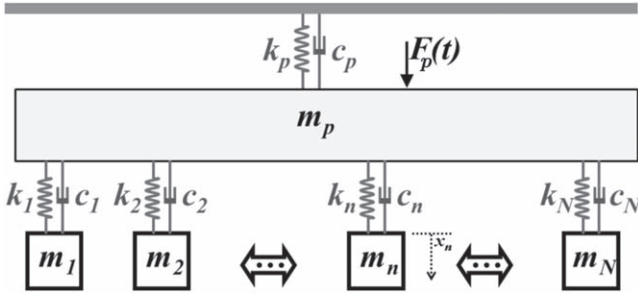


Figure 1. Array of single degree of freedom oscillators attached to a host structure [11, 15, 16].

structure. By doing so, a bandgap is created in the frequency response of the host structure. Since the study of these systems is a relatively recent innovation, most of the relevant studies have been focused on analyzing the basic effect of metamaterials in the frequency domain, analyzing the limiting behavior, or on optimizing the placement of the piezoelectric oscillators on the host structure. Issues like robustness or sensitivity to perturbation in the location or the parameters of the piezoelectric oscillators are yet to be fully understood. Furthermore, the host systems considered in most of the relevant studies are monolithic beams, plates, or shell structures. Because of the nature of the problem of synthesizing metamaterials, it is reportedly more difficult to generalize the synthesis of metamaterial structures to arbitrary geometry. This can be attributed to the fact that metamaterials rely heavily on the periodicity of the substructures which can be hard to define in complex structures. Theoretically, the governing equations of metamaterials systems and PSOs look very similar. However, there are significant differences in the models as well as in the intended goals of the overall system after synthesis. One primary difference is that substructures are generally identical in metamaterials, whereas, parameter distributions dictate the mix of material properties of the piezoelectric substructures in PSOs. Metamaterials create bandgaps by essentially moving existing resonant peaks outside of the frequency band of interest. Whereas PSOs extend the effect of DVAs to cancel an existing resonant peak in the frequency response. This implies that modal spillover is very minimal in case of PSOs as opposed to that of metamaterials. However, it is important to note that the frequency band of metamaterial systems are typically larger (spanning over multiple resonant peaks), and sometimes much larger, than that of the PSOs.

3. Subordinate oscillator arrays

Figure 1 shows a simple SOA, consisting of N mass-spring-damper oscillators, attached to a host structure of mass m_p , stiffness k_p , damping c_p and natural frequency ω_p [11, 15, 16]. The mass, stiffness and the damping of the n th oscillator in the SOA are denoted by m_n , k_n and c_n , respectively. Since the PSO approach used in this paper is very similar to the one used in [11], a brief summary of relevant theory is presented here. Vignola *et al* [11] derived a closed form equation for the

frequency response function (FRF) of the map from the applied external force F_p to motion of the primary x_p . The frequency response at a given nondimensional frequency Ω can be calculated using the function

$$\frac{X_p(\Omega)k_p}{F_p(\Omega)} = \left(1 - \Omega^2 + \frac{i\Omega}{Q_p} + \sum_{n=1}^N \alpha_n \left(\frac{-\Omega^2 \left(1 + \frac{i\Omega}{\beta_n Q_n} \right)}{1 - \left(\frac{\Omega}{\beta_n} \right)^2 + \frac{i\Omega}{\beta_n Q_n}} \right) \right)^{-1}, \quad (1)$$

where

$$\Omega := \omega/\omega_p, \quad \alpha_n := \frac{m_n}{m_p}, \quad \beta_n := \sqrt{\frac{\gamma_n}{\alpha_n}}, \\ \gamma_n := \frac{k_n}{k_p}, \quad Q_n := \frac{\sqrt{m_n k_n}}{c_n}. \quad (2)$$

In equations (1) and (2), the subscript p represents the properties of the primary or host structure, and the subscript n represents the properties of the n th attached substructure. The variable β_n is the nondimensional frequency of each substructure in the SOA. It can be expressed in terms of the nondimensional mass α_n and the nondimensional stiffness γ_n as shown in equation (2). The constants Q_n and Q_p are the quality factors of the substructure and the host structure, respectively. From equation (1), it is evident that the frequency response of the host structure attached to an SOA depends on the distributions of the nondimensional mass, stiffness and frequency denoted by α_n , γ_n and β_n , respectively. This implies that the problem of designing an SOA amounts to a problem of selecting three distributions instead of $3N$ parameters for all the substructures. The interdependence of α_n , β_n and γ_n implies that we have to construct distributions for only two of the three terms.

3.1. Nondimensional frequency distributions

As mentioned earlier, the design of a flat frequency response using SOAs distributes the frequency band of the SOA around the host structure's natural frequency. This is achieved by assigning an appropriate distribution to the nondimensional frequency β_n . The distribution used in [11] for β_n is represented by equations of the form

$$\beta_n = \begin{cases} \frac{\Delta}{2} \left(\left(\frac{2(n-1)}{N-1} \right)^p - 1 \right) + 1 & \text{for } n \leq \frac{N}{2}, \\ \frac{\Delta}{2} \left(1 - \left(\frac{2(N-n)}{N-1} \right)^p \right) + 1 & \text{for } n \geq \frac{(N+1)}{2}. \end{cases} \quad (3)$$

The nondimensional frequency distribution defined by equation (3) is an antisymmetric curve centered at 1. The parameter Δ in equation (3) represents the bandwidth of the nondimensional frequency distribution. Figure 2 shows the frequency response of the host structure for various values of Δ . The parameter p determines how the substructures are spaced around the center. When $p = 1$, the frequency of the substructures are equally spaced around the natural frequency of the host structure. When $p = 0$, the host structure is

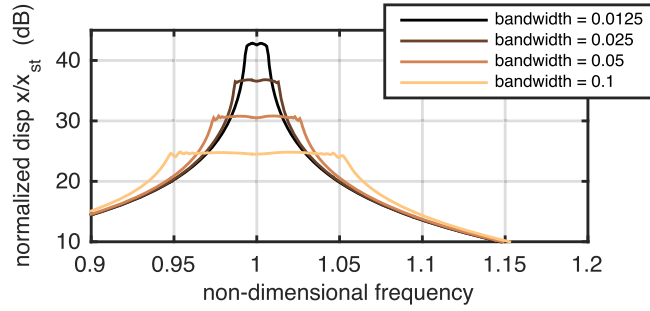


Figure 2. Broadband flat attenuation by SOA for varying bandwidths [16].

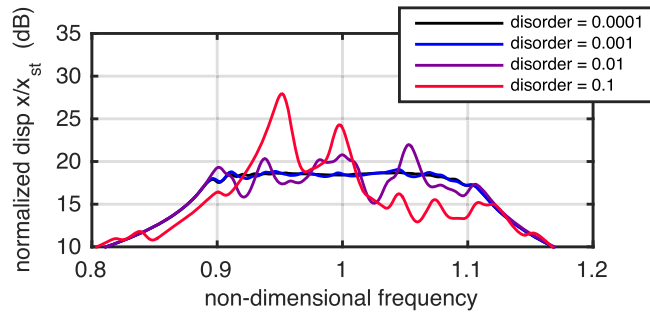


Figure 3. Degradation of SOA's performance with disorder [16].

attached to a DVA whose nondimensional frequency is 1. Finally, $p = \infty$ corresponds to case where the host structure is attached to two DVA's with nondimensional frequencies equal to $1 - \Delta/2$ and $1 + \Delta/2$. Later in this paper, it will be shown that a nondimensional frequency distribution as expressed in equation (3) can be used to design a PSOA.

3.2. Effect of disorder on performance of SOAs

Disorder or parameter uncertainties in systems can be induced due to fabrication errors in substructures or measurement errors in structural properties of the host. Vignola *et al* [16] studied the effect of disorder on the frequency response of a primary structure attached to an SOA. Figure 3 shows the degradation of SOA's performance as the disorder is increased. The figure shows a flat frequency response when uncertainty is low and a non-flat response as uncertainty approaches 0.1. These results indicate that SOA's desired performance is limited by the precision of manufacturing and accuracy of measurements of the host's structural properties. One possible solution to overcome some of these issues is to develop a tunable SOA, a PSOA, which potentially allows for effective change of structural properties after fabrication.

4. Host structure with PSOA model

In this section, the \mathcal{H} variational principle which is based on extremization of the electric enthalpy and is discussed in appendix A.1, will be used to model a PSOA attached to a host structure. The canonical PSOA consists of a series of

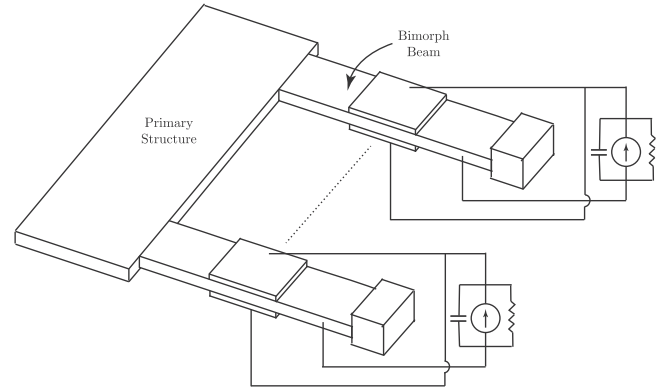


Figure 4. A PSOA attached to a host structure.

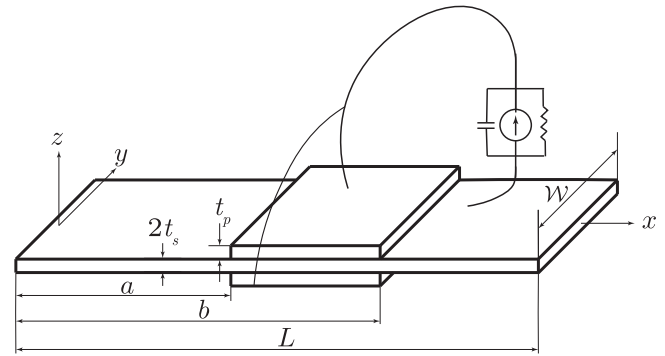


Figure 5. Dimensions of a substructure in a PSOA.

bimorph beams with shunt circuits connected to them. The shunt circuit of k th bimorph beam in the array consists of a resistor R_k , capacitor C_k and current source i_k in parallel. Starting with a distributed beam model, finite dimensional approximations are introduced. Ultimately each oscillator in the PSOA is modeled as a single degree of freedom system. Figure 4 shows a piezoelectric subordinate array attached to a host structure. The dimensions of each appendage in the PSOA are shown in figure 5. The host structure is assumed to have two inputs, base motion \mathfrak{z} and applied force F_p .

If x_p represents the absolute motion of the primary structure and w_i is the relative motion of appendage i in a PSOA with N substructures, the kinetic energy of the system shown in figure 4 can be expressed as

$$T = \underbrace{\frac{1}{2}m_p(\dot{x}_p - \dot{\mathfrak{z}})^2}_I + \sum_{i=1}^N \left\{ \underbrace{\frac{1}{2} \int_0^{L_i} \rho_i A_i \left(\dot{x}_p + \frac{\partial w_i}{\partial t} - \dot{\mathfrak{z}} \right)^2 dx_i}_II + \underbrace{\frac{1}{2}m_i \left(\dot{x}_p + \frac{\partial w_i}{\partial t}(t, L_i) - \dot{\mathfrak{z}} \right)^2}_III \right\}, \quad (4)$$

where ρ_i , A_i and L_i are the density, cross sectional area and length of the bimorph, respectively. The cross sectional area

is defined as $A_i := 2t_{s,i} \cdot \mathcal{W}_i$, where $2t_{s,i}$ and \mathcal{W}_i are the thickness and width of the substrate as shown in figure 5, respectively. Further, m_i is the tip mass attached to the bimorph, and m_p is the host structure's mass. The terms I, II and III in equation (4) represent the kinetic energy contributions from the primary mass of the host structure, distributed mass of each appendage in the SOA and tip mass of each appendage in the SOA respectively.

After following the steps shown in appendix B, the kinetic energy can be expressed in the quadratic form

$$T = \frac{1}{2} \{ \dot{\mathbf{W}}_1^T \cdots \dot{\mathbf{W}}_n^T | (\dot{x}_p - \dot{\mathfrak{z}}) \} \times \begin{bmatrix} \mathbf{M}_{11} & \cdots & \mathbf{0} & \mathbf{M}_{1p} \\ \vdots & \ddots & \vdots & \vdots \\ \mathbf{0} & \cdots & \mathbf{M}_{nn} & \mathbf{M}_{np} \\ \hline \mathbf{M}_{1p}^T & \cdots & \mathbf{M}_{np}^T & \mathbf{M}_{pp} \end{bmatrix} \times \begin{Bmatrix} \dot{\mathbf{W}}_1 \\ \vdots \\ \dot{\mathbf{W}}_n \\ \hline (\dot{x}_p - \dot{\mathfrak{z}}) \end{Bmatrix}, \quad (5)$$

where the vectors $\mathbf{W}_1, \dots, \mathbf{W}_n$ is defined as the vector of temporal components of the Galerkin approximation $w_i(x, t) = \sum_{j=1}^n \Psi_{ij}(x) W_{ij}(t) = \Psi_i^T(x) \mathbf{W}_i(t)$. The terms $\mathbf{M}_{11}, \dots, \mathbf{M}_{nn}, \mathbf{M}_{1p}, \dots, \mathbf{M}_{np}$ and \mathbf{M}_{pp} are defined in appendix B.

In order to derive an expression for the electromechanical potential, we first derive a representation for the electric enthalpy density. The linear electric enthalpy density of each appendage is calculated from the following expression in [82]

$$\mathcal{H}_i := \frac{1}{2} C_i^E S_i^2 - e_i S_i E_i - \frac{1}{2} \epsilon_i^S E_i^2, \quad (6)$$

where E_i is the electric field, C_i^E is the material stiffness at constant electric field, $S_i := -z_i \frac{\partial^2 w_i}{\partial x_i^2}$ is the axial strain in a Bernoulli–Euler beam, e_i is the piezoelectric constant, ϵ_i^S is the permittivity of the piezoelectric material at constant strain. After substituting the expression for electric enthalpy density into equation (A.3), the total electromechanical potential of a PSOA attached to a host structure will have the form

$$\mathcal{V}_{\mathcal{H}} := \underbrace{\frac{1}{2} K_p x_p^2}_{\text{IV}} + \sum_{i=1}^N \underbrace{\mathcal{V}_{\mathcal{H}_i}}_{\text{V}} \quad (7)$$

In the above equation, term IV represents the strain energy of the host structure's spring with stiffness K_p . Further, term V represents the electromechanical potential of each piezoelectric oscillator in the PSOA and is expressed in the form

$$\mathcal{V}_{\mathcal{H}_i} = \frac{1}{2} \mathbf{W}_i^T \mathbf{K}_{ii} \mathbf{W}_i - \mathbf{B}_i^T \mathbf{W}_i V_i - \frac{1}{2} D_i V_i^2 - \frac{1}{2} C_i V_i^2, \quad (8)$$

Here, D_i is the effective capacitance of the piezoelectric material, C_i is the shunt capacitance, \mathbf{B}_i^T is the control influence matrix and V_i is the voltage across the shunt circuit. The intermediate steps that lead to the above expression are discussed in appendix C. The virtual work done by the non-conservative electromechanical loads will have contributions from the force input, current source, resistor and damping in

the system. The virtual work done is expressed in the form

$$\delta W_{nc} = F_p \delta(x_p - \mathfrak{z}) + \sum_{k=1}^N i_k \delta \lambda_k - \sum_{k=1}^N \frac{\dot{\lambda}_k}{R_k} \delta \lambda_k + \delta W_{nc,visc}, \quad (9)$$

where λ_k is the flux linkage across the shunt circuit, i_k is the current source in the shunt circuit, R_k is the resistor in the shunt circuit and F_p is the force applied to primary mass m_p . The virtual work done by mechanical damping can be derived from $\delta W_{nc,visc} = \delta \mathbf{q}^T \mathcal{Q}_{visc}$, where \mathcal{Q}_{visc} is the generalized forces of viscous damping and \mathbf{q} is the set of generalized coordinates defined by the vector

$$\mathbf{q} = \{ \mathbf{W}_1^T \ \mathbf{W}_2^T \ \dots \ \mathbf{W}_N^T \ x_p \}^T.$$

The generalized forces due to damping \mathcal{Q}_{visc} can be derived from the expression $\mathcal{Q}_{visc} = -\frac{\partial \mathcal{F}}{\partial \dot{\mathbf{q}}}$ where

$$\mathcal{F} := \dot{\mathbf{q}}^T \underbrace{\begin{bmatrix} \mathbb{C} & \mathbf{0} \\ \mathbf{0}^T & C_p \end{bmatrix}}_{\mathbf{C}} \dot{\mathbf{q}} \quad (10)$$

is the Rayleigh dissipation function. In equation (10), C_p is the damping of the primary structure and $\mathbb{C} := \text{diag}(C_{11}, C_{22}, \dots, C_{NN})$, where C_{nn} is the damping matrix of the n th oscillator in the PSOA. After simplification, the virtual work done by the viscous damping will have the form

$$\delta W_{nc,visc} = -\delta \mathbf{q}^T \mathbf{C} \dot{\mathbf{q}}. \quad (11)$$

The equations of motion is obtained, as discussed in appendix D, by using the \mathcal{H} Variational Principle. The most general finite dimensional model is then given by

$$\begin{bmatrix} \mathbf{M} & \mathbf{M}_p \\ \mathbf{M}_p^T & M_{pp} \end{bmatrix} \begin{Bmatrix} \ddot{\mathbf{W}} \\ \ddot{x}_p \end{Bmatrix} + \begin{bmatrix} \mathbb{C} & \mathbf{0} \\ \mathbf{0}^T & C_p \end{bmatrix} \begin{Bmatrix} \dot{\mathbf{W}} \\ \dot{x}_p \end{Bmatrix} + \begin{bmatrix} \mathbb{K} & \mathbf{0} \\ \mathbf{0}^T & K_p \end{bmatrix} \begin{Bmatrix} \mathbf{W} \\ x_p \end{Bmatrix} - \begin{bmatrix} \mathbb{B} \\ \mathbf{0} \end{bmatrix} \mathbb{V} = \begin{Bmatrix} \mathbf{0} \\ \hat{F}_p \end{Bmatrix}, \quad (12)$$

where $\hat{F}_p = F_p + M_{pp} \ddot{\mathfrak{z}}$ and

$$\mathbb{B}^T \dot{\mathbf{W}} + \mathbb{D} \dot{\mathbf{V}} + \zeta \dot{\mathbf{A}} - \dot{\mathbf{i}} + \mathbf{C} \dot{\mathbf{V}} = \mathbf{0}. \quad (13)$$

It should be noted that this equation of motion allows for the possibility of multi-mode approximations of each PSOA appendage.

Also, as a part of comparison, it is known that the actuator equations for a monolithic, distributed, linear piezoelectric composite (such that those that arise from piezoelectric beams, plates, or shells (see [12])) has the form

$$\mathbf{M}_{mono} \ddot{\mathbf{W}} + \mathbf{C}_{mono} \dot{\mathbf{W}} + \mathbf{K} \mathbf{W} = \mathbb{B}_{mono} \mathbb{V}$$

with \mathbf{M}_{mono} , \mathbf{C}_{mono} , \mathbf{K}_{mono} symmetric, sparse and banded. However, these matrices are not guaranteed to have the block zero structure of equation (12). As mentioned in the introduction, it may be possible using component mode synthesis to drive the equation to a similar form. It we can choose

$\mathbb{W} = [\mathbb{W}_I^T \mathbb{W}_D^T]^T = [\Psi_I^T \Psi_D^T]^T$ where $[\Psi_I \Psi_D] \mathbb{K} [\Psi_I^T \Psi_D^T]^T = \text{diag}(K_{II}, K_{DD})$ and $[\Psi_I \Psi_D] \mathbb{C} [\Psi_I^T \Psi_D^T]^T = \text{diag}(C_{II}, C_{DD})$, then the more general equation can be cast in a form somewhat similar to equation (12). However, this definition can result in new, nonintuitive definitions of states.

5. PSOA design using frequency response function

In this section, the closed form FRF from the input force F_p to the displacement x_p of the host structure is derived when each subordinate element is modeled with a single degree of freedom. Next, various strategies that can be implemented in the design of the PSOA are discussed. As it will become evident in the current section, the resistor and the current source in the shunt circuit are not necessary for passive PSOAs designed for vibration attenuation. The values R^{-1} and i are assumed to be zero in the subsequent calculations. Further, it is assumed that there is no base excitation to simplify the derivation of the closed-form expression. After making use of these assumptions, integrating equation (13) with zero initial conditions generates an expression for voltage of the form

$$\mathbb{V} = -(\mathbb{D} + \mathbb{C})^{-1} \mathbb{B}^T \mathbb{W}. \quad (14)$$

Substituting the expression for voltage into equation (12) and taking the Laplace transform will result in the expression

$$\begin{bmatrix} \mathbb{M}s^2 + \mathbb{C}s + \hat{\mathbb{K}} & \mathbb{M}_p s^2 \\ \mathbb{M}_p^T s^2 & M_{pp} s^2 + C_p s + K_p \end{bmatrix} \begin{Bmatrix} \mathbb{W} \\ x_p \end{Bmatrix} = \begin{bmatrix} \mathbf{0} \\ f_p(s) \end{bmatrix}, \quad (15)$$

where

$$\hat{\mathbb{K}} := \mathbb{K} + \mathbb{B}(\mathbb{D} + \mathbb{C})^{-1} \mathbb{B}^T. \quad (16)$$

It is evident from the expression for $\hat{\mathbb{K}}$ that the shunt capacitance induces a change in the stiffness of the PSOA. As shown in appendix E, the FRF can be obtained by evaluating this transfer function along the imaginary axis, i.e. by substituting $s = i\omega$. The nondimensionalized frequency response function, obtained by dividing both sides of equation (E.6) by the stiffness of the host structure K_p , is expressed as

$$\frac{x_p K_p}{f_p} = \left[1 - \Omega^2 + \frac{i\Omega}{Q_p} + \sum_{n=1}^N \hat{\alpha}_n \left[\Omega^2 + \frac{-\Omega^2 \left(1 + \frac{i\Omega}{\beta_n Q_n} \right)}{1 - \left(\frac{\Omega}{\beta} \right)^2 + \frac{i\Omega}{\beta_n Q_n}} \right] \right]^{-1}, \quad (17)$$

where

$$\begin{aligned} \Omega &= \omega \sqrt{\frac{M_{pp}}{K_p}}, & \tilde{\alpha}_n &= \frac{M_{nn}}{M_{pp}}, \\ \beta_n &= \sqrt{\frac{\gamma_n}{\tilde{\alpha}_n}}, & \gamma_n &= \frac{\hat{K}_{nn}}{K_p}, \\ Q_n &= \frac{\sqrt{M_{nn} \hat{K}_{nn}}}{C_{nn}}, & \hat{\alpha}_n &= \alpha_n^2 \tilde{\alpha}_n. \end{aligned} \quad (18)$$

The definitions of M_{nn} , C_{nn} , K_{nn} and α_n are available in appendix E. Equation (17) is a principal result for electromechanical systems in this paper and should be compared to equation (1) for purely mechanical systems.

5.1. Methodology for PSOA design

As discussed in the earlier sections, flat broadband attenuation of frequency response can be achieved when the bandwidth of the SOA is distributed around the host structure's natural frequency. The SOA bandwidth is defined as the range of isolated natural frequencies from the smallest possible resonant frequency to the largest resonant frequency. In this subsection, two systematic approaches to achieve the good designs will be discussed. The equations of motion of piezoelectric oscillator n in the PSOA can be extracted from equations (12) and (13). They have the form

$$M_{nn} \ddot{W}_n + C_{nn} \dot{W}_n + K_{nn} W_n - B_n V_n = -M_{np} \ddot{x}_p, \quad (19)$$

$$B_n^T \dot{W}_n + (D_n + C_n) \dot{V}_n + \frac{V_n}{R_n} - i_n = 0. \quad (20)$$

As mentioned at the beginning of this section, the shunt circuit consists of only a capacitor for each appendage. Hence, the terms corresponding to resistor and current source in equations (20) can be set to zero. Further, using single mode approximation simplifies the vectors M_{nn} , M_{np} , C_{nn} , K_{nn} , B_n and W_n in equations (19) and (20) to scalars M_{nn} , M_{np} , C_{nn} , K_{nn} , B_n and W_n , respectively. With these assumptions, equations (19) and (20) simplify to

$$M_{nn} \ddot{W}_n + C_{nn} \dot{W}_n + K_{nn} W_n - B_n V_n = -M_{np} \ddot{x}_p, \quad (21)$$

$$B_n \dot{W}_n + (D_n + C_n) \dot{V}_n = 0. \quad (22)$$

Assuming zero initial conditions, equation (22) can be integrated and rewritten as an expression for voltage of the form

$$V_n = -\frac{B_n}{D_n + C_n} W_n. \quad (23)$$

Substituting the expression for voltage into the equation (19) results in

$$M_{nn} \ddot{W}_n + C_{nn} \dot{W}_n + \left[K_{nn} + \frac{B_n^2}{D_n + C_n} \right] W_n = -M_{np} \ddot{x}_p. \quad (24)$$

For a system represented by a second order differential equation as shown in equation (24), the natural frequency will be

$$\omega_n = \sqrt{\frac{K_{nn} + \frac{B_n^2}{D_n + C_n}}{M_{nn}}} = \sqrt{\frac{\hat{K}_{nn}}{M_{nn}}}. \quad (25)$$

Equation (25) gives the isolated natural frequency of an oscillator in a PSOA. The system parameters M_{nn} , K_{nn} , B_n , D_n and C_n of each oscillator are chosen in such a way that the PSOA achieves the desired bandwidth. The following paragraphs discuss two specific strategies for making these choices.

5.2. Design by tip mass distribution

The first approach varies the tip mass to achieve the necessary natural frequency distribution. After fixing all the parameters except tip mass, the nondimensional mass distribution $\tilde{\alpha}_n$ can be calculated using the relation given in equation (18). The nondimensional mass of oscillator n is

$$\tilde{\alpha}_n := \frac{\gamma_n}{\beta_n^2} := \frac{M_{nn}}{M_{pp}} = \frac{\mathcal{M}_{nn} + m_{nn}}{m_p + \sum_i (\mathcal{M}_i + m_i)}, \quad (26)$$

which can be rearranged as

$$\begin{aligned} m_1 + m_2 + \dots + \left(1 - \frac{\Psi(L)^2}{\tilde{\alpha}_i}\right) + \dots + m_N \\ = \frac{\int_0^L \rho A \Psi(x)^2 dx}{\tilde{\alpha}_i} - (m_p + N\rho AL). \end{aligned} \quad (27)$$

The tip mass distribution that can achieve the desired frequency distribution can be calculated using the relation

$$\mathbf{m} = (I_N - P)^{-1}Q, \quad (28)$$

with

$$\begin{aligned} P := \text{diag}\left(\frac{\Psi(L)_1^2}{\tilde{\alpha}_1}, \frac{\Psi(L)_1^2}{\tilde{\alpha}_2}, \dots, \frac{\Psi(L)_1^2}{\tilde{\alpha}_N}\right) \text{ and} \\ Q := \begin{bmatrix} \left(\frac{\int_0^L \rho A \Psi(x)^2 dx}{\tilde{\alpha}_1} - (m_p + N\rho AL)\right)^T \\ \vdots \\ \left(\frac{\int_0^L \rho A \Psi(x)^2 dx}{\tilde{\alpha}_N} - (m_p + N\rho AL)\right)^T \end{bmatrix}. \end{aligned} \quad (29)$$

5.3. Design by capacitance distribution

The second approach specifies stiffness properties by varying shunt capacitance while fixing the other parameters. Similar to the first approach, all parameters except the shunt capacitance are kept constant. The nondimensional stiffness of oscillator n

$$\gamma_n := \beta_n^2 \tilde{\alpha}_n := \frac{\hat{K}_{nn}}{K_p}. \quad (31)$$

The shunt capacitance of oscillator n that can produce the required nondimensional frequency can be calculated using

the relation

$$C_n = \frac{B_n^2}{\hat{K}_{nn} - K_{nn}} - D_n. \quad (32)$$

The advantages and the limitations of both the approaches will be discussed along with the numerical results in section 7.1.

6. Experimental procedure

Performance of PSOAs in attenuating resonant peaks was tested on an aluminum beam shown in figure 6. The aluminum beam of dimensions 29.7 cm × 7.67 cm × 1.275 cm ($l \times w \times t$) was clamped at one end, while the bimorphs were attached at its free end. A shaker was attached to the beam at a distance of 13.2 cm from its tip. The frequency response functions of the structure were evaluated between the input force measured by a PCB dynamic force transducer and the tip-velocity measured with a single point laser vibrometer (PSV-100). The attenuation in the resonant peaks of the aluminum beam was monitored from the FRFs measured with an LMS SCADAS DAQ system. Initially, baseline FRF of the host structure (without PSOA) was recorded, which was later compared to FRFs of the modified structure as piezoceramic bimorphs (Part Number: T226-H4-503Y) were attached to it in succession. The material and geometric properties of these PSOAs are summarized in tables 2 and 3. Even though the bimorphs have an aspect ratio that resembles a rectangular plate rather than a beam, the fundamental frequency of the cantilevered bimorphs is the only resonant frequency in the bandwidth of interest. Therefore, each PSOA can be considered as a tuned single degree-of-freedom dynamic oscillator.

The performance of four PSOAs, each with 2, 4, 6, 8 bimorphs, was studied during the experiments. The natural frequencies of the bimorphs in the PSOAs were estimated from the FRFs between the base acceleration and the tip velocity of the bimorph attached to the host structure. For these experiments, the length of the bimorphs was varied to achieve the desired frequency distribution and tip masses were only added once the maximum length of bimorphs was reached. Because of the geometry of the PSOA, it was not possible to vary tip mass alone: the size of the tip masses would interfere with one another. Thus, the practical constraints in the setup play a critical role in determining the parameters that can be varied to achieve the desired non-dimensional frequency distribution. Theoretically, the length and the tip mass variation should be sufficient to tune the natural frequencies of the bimorphs. However, due to uncertainties in the experiments, the length was fixed first, the tip-mass (if required) was added next, and finally, the shunt capacitance was tuned to approach the desired natural frequency.

Furthermore, the performance of the PSOAs with open shunt circuits was evaluated under varying dynamic properties of the host structure. Once a tip-mass was added to the

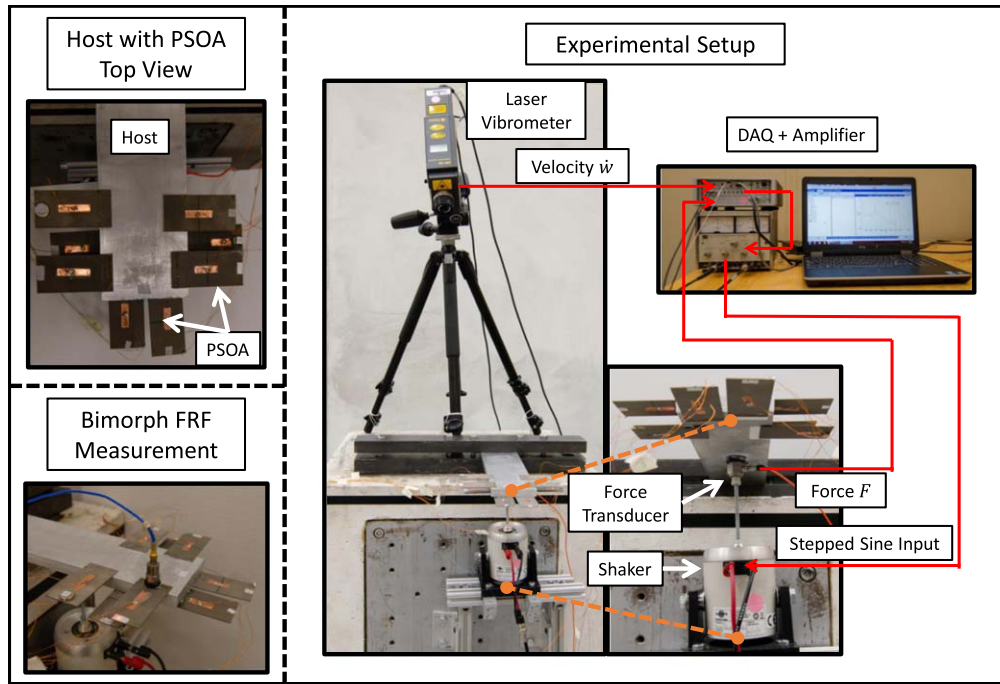


Figure 6. Experimental setup.

Table 2. Parameters of PSOAs used in the experiments.

No.	No. of bimorphs	Mass ratio	Bimorph ref. (figure 17)	Length (mm)	Tip-mass (g)	Shunt capacitance	Natural frequency (Hz)
1	2	2.30%	A, B	53.28, 48.88	0, 0	220 nF, 220 nF	110.25, 123.5
2	4	4.59%	C, A B, D	55.70, 53.28, 48.88, 46.24	0, 0, 0, 0	470 nF, 820 nF, 220 nF, O	94, 108.5, 123.5, 136.5
3	6	7.13%	E, C, A, B, D, F	58.5, 55.70, 53.28, 48.88, 46.24, 44.45	1.75, 0, 0, 0 0, 0	470 nF (BS), 220 nF, 220 nF, 220 mF, 220 mF, O	86.25, 95, 110.25, 119 130.75, 142.75
4	8	9.87%	G, E, C, A, B, D, F, H	58.50, 58.50, 55.70, 53.28, 48.88, 46.24, 44.45, 42.85	3.72, 1.75, 0, 0 0, 0 0, 0	O, O, O, 220 nF, 2.2 mF, C, O, 2.2 mF	79.75, 94, 97.25, 110.25 122.25, 130.75 142.75, 150

Note. (BS)—capacitance between bottom piezo layer and substrate (top piezo layer is not included in the circuit), O—shunt circuit is open, C—shunt circuit is closed.

Table 3. Properties of bimorphs used in experiments.

Bimorph properties	
Substrate material	Brass
Total mass	10.3 (g)
W_i	31.75 (mm)
$t_{p,i}$	0.27 (mm)
$2t_{s,i}$	0.11 (mm)

host, the PSOAs were then re-tuned using the shunt capacitances. The performance recovery achieved by the PSOAs after shunt tuning was studied for three different tip masses, 31.60, 62.81, and 81.29 g. The results of the above-mentioned experiments are discussed in section 8.

7. Numerical results

We simulated the response of the host structure attached to the PSOAs that were designed using approaches presented in the previous sections under ideal as well as non-ideal conditions. To better contrast the simulation results for different cases, the host's structural properties, the nondimensional frequency distribution β_n , the number of substructures N in the PSOA, and majority of the fixed parameters of the PSOA were maintained constant for all simulations. The host structure was assumed to have a mass $m_p = 1000$ kg, stiffness $K_p = 1\,273\,300$ N m⁻¹ and a very low damping ratio $\zeta_p = 0.000\,1$, which places its natural frequency at 35.68 rad s⁻¹. The nondimensional frequency distribution β_n shown in figure 7 was used for the simulations and was

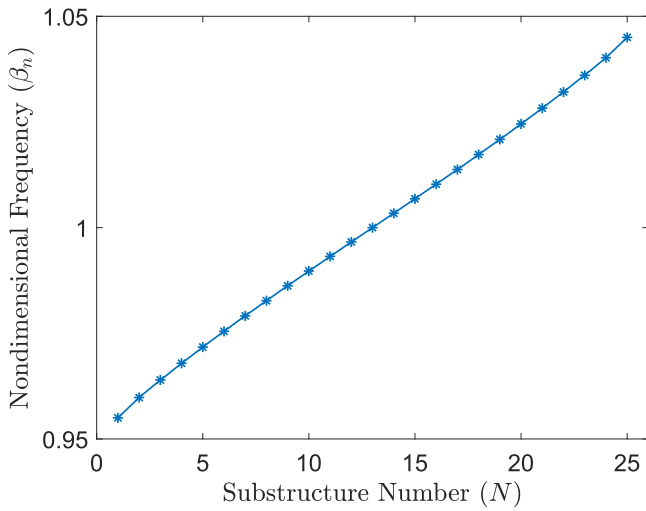


Figure 7. Nondimensional frequency distribution obtained using equation (3) with $\Delta = 0.09$ and $p = 0.9$.

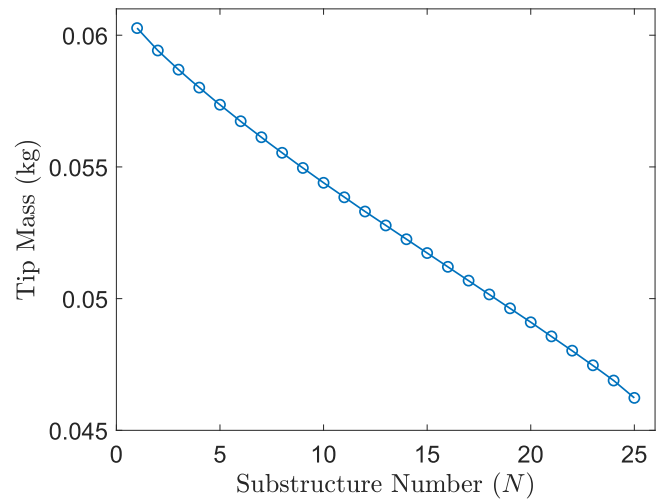


Figure 9. Tip mass distribution used to achieve the frequency response shown in figure 8.

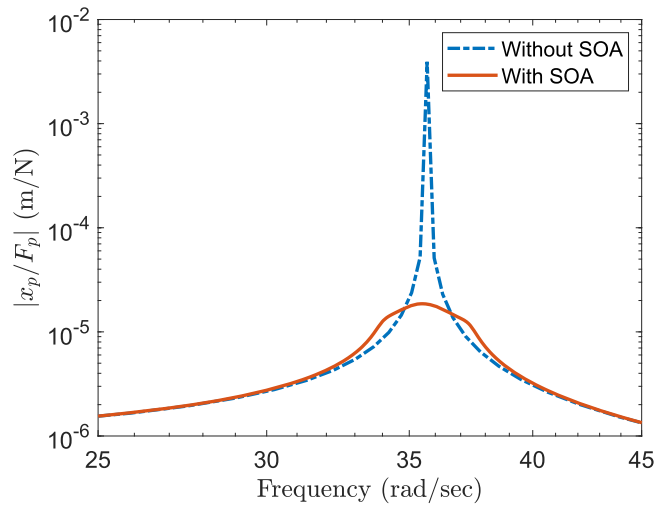


Figure 8. Frequency response function from force input F_p to displacement x_p of a host structure with and without a PSOA. The PSOA was designed using first approach.

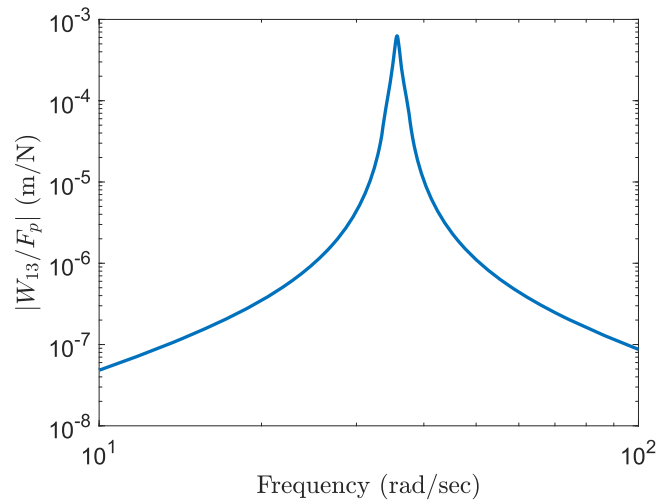


Figure 10. Frequency response function from force applied F_p on the host structure to the displacement W_{13} of the 13th substructure in the PSOA designed using first approach.

generated using equation (3) with $\Delta = 0.09$ and $p = 0.9$. We assigned the following values to the fixed parameters of the SOA: $C = 6.9e + 10$ Pa, $\rho_m = 2.3e + 3$ kg m⁻³, $N = 25$, $L = 0.5$ m, $\mathcal{W} = 0.025$ m, $2t_s = 0.003$ m, $a = 0.25$ l, $b = 0.75$ l, $e_{31} = -10.4$ C m⁻², $\epsilon = 13.3$ nF m⁻¹, $\zeta_{\text{SOA}} = 0.01$. In the following subsections, we will discuss the results we obtained for the various simulation cases.

7.1. PSOA simulations under ideal conditions

In the first set of simulations, we assumed that we had perfect knowledge of host structural properties, and the fabricated PSOA adhered strictly to the design specifications.

When we simulated the effect of PSOA designed using the first approach on the host structure, we obtained the frequency response shown in figure 8. This result was obtained for a piezoelectric patch thickness of $t_p = 0.0005$ m. As the

figure portrays, the addition of the PSOA reduces the steady state displacement of the host structure to approximately 1% of its actual steady state displacement at the resonant frequency. This result indicates that PSOAs can indeed achieve a reasonably flat bandwidth in the host structure's resonant peak region. Figure 8 also shows that the magnitude increase outside this region is negligible. Figure 9 shows the tip mass distribution that achieved the flat bandwidth shown in figure 8. This is a substantial qualitative improvement over a classical DVA.

One of the critical aspects to consider during the design of SOAs, as well as the DVAs, is the maximum displacement of the substructures. We plotted the frequency response from the force input F_p to the displacement of the 13th substructure W_{13} , which can be seen in figure 10. As evident from the figure, to ensure the displacement is within the mechanical

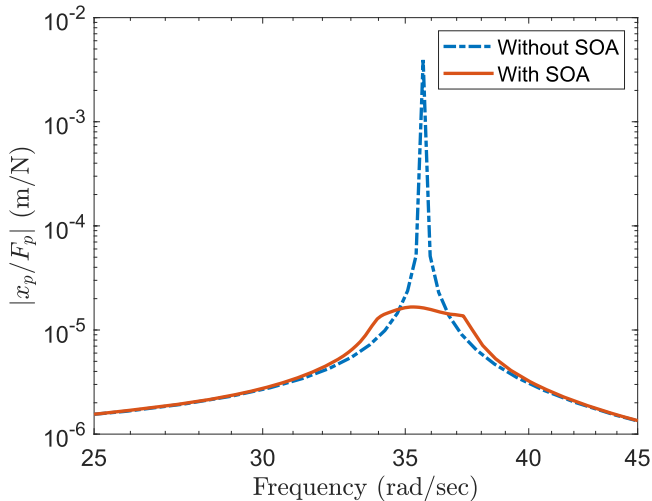


Figure 11. Frequency response function from force input F_p to the displacement of the host structure attached to a PSOA designed using second approach.

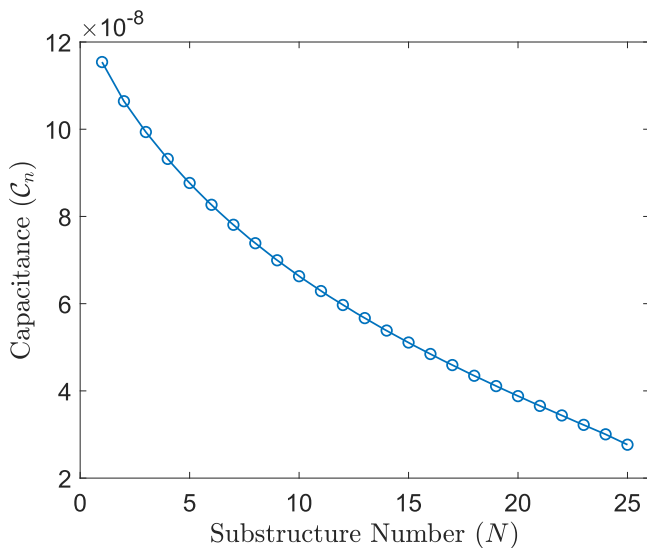


Figure 12. Capacitance distribution used to achieve the frequency response shown in figure 11.

limitations, the maximum force input to the host structure should not exceed 10^3 times the maximum displacement allowable in the substructure.

In the second set of simulations, we tested a PSOA designed using a distribution of capacitive shunts. We calculated the total tip mass of each substructure to be $m_i = 0.06944$ kg from the prescribed total mass ratio $\mu = 4.065 \times 10^{-3}$. Assuming the piezoelectric thickness as $t_p = 0.003$ m, we obtained the capacitance distribution shown in figure 12. Figure 11 shows the frequency response of the host structure when the shunt capacitors followed the distribution shown in figure 12. The primary implication of this result is that it is possible to achieve flat attenuation using mechanically identical oscillators. One of the advantages of using a capacitive shunt distribution is that it allows the

designer to impose a mass ratio. Prescribing an actual mass ratio is problematic in the first approach since the tip masses are unknown during the initial stages of design. Hence, design using the first approach requires an iterative process. On the other hand, it is important to note that the PSOAs designed using the second approach usually require piezoelectric patches whose thicknesses are no longer negligible. In such cases, the model developed using modal shape functions is interpreted as an approximation whose accuracy must be validated. In some instances, individual variations of tip-mass or the capacitance are not sufficient to generate the necessary nondimensional frequency distribution. In such cases, multiple parameters must be simultaneously varied as shown in the experimental results.

7.2. PSOA simulations under non-ideal conditions

In the previous subsection, we demonstrated the effectiveness and the advantages of the PSOAs through simulations. But the simulations relied on ideal conditions which entailed perfect knowledge of the host structure's properties and a high level of precision during manufacturing. These assumptions may not be justified in some applications. Further, the structural properties of some systems can degrade or evolve over time which can render the SOA ineffective. In this subsection, we will discuss the performance of the PSOAs under non-ideal conditions and analyze the robustness of PSOA systems in the presence of disorder. In the following set of discussions, we restrict our analysis to the PSOA designed using the first approach. The piezoelectric patch thickness value used for this set of simulations is $t_p = 0.001$ m.

Assume that the host's structural properties used in the previous simulations are inaccurate and the actual host structure has a stiffness which is 10% less than what we measured. Figure 13 shows the effect of this error on the frequency response of the host. The PSOA, which has no capacitive shunt, is expected to generate a flat frequency response. However, the presence of error in host structure model induces a peak in the frequency response as shown in figure 14. The induced peak disappeared, when we attached the PSOA with shunts of capacitance $C_n = 1$ F. As can be seen in figure 14, we were able to achieve a frequency response very similar to the expected response after shunt tuning.

Similarly, let us assume that the fabricated PSOA designed in section 7.1 did not comply with the design specifications. To imitate this disparity in the design and fabricated SOA's parameters, we introduced a -10% error in the stiffness \mathbb{K} of the SOA. The ideal PSOA that we designed in section 7.1 attached to a shunt capacitance of $C_n = 1$ F would have produced a spectrally flat response as shown in figure 15. However, the fabrication errors induce a peak in the frequency response as shown in the same figure. After reducing the shunt capacitance to $C_n = 1e-9$ F, we were able to achieve a frequency response that almost mimics the expected response.

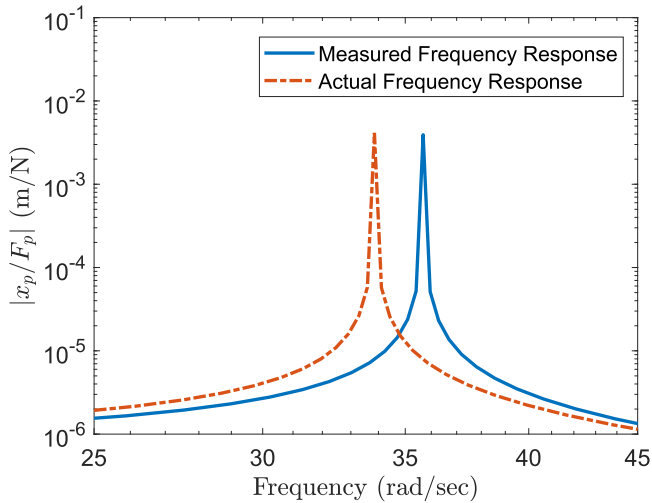


Figure 13. Frequency response function from the force applied F_p to the displacement x_p of the host structure. Effect of 10% disorder in host structure’s stiffness on the natural frequency can be seen in this plot.

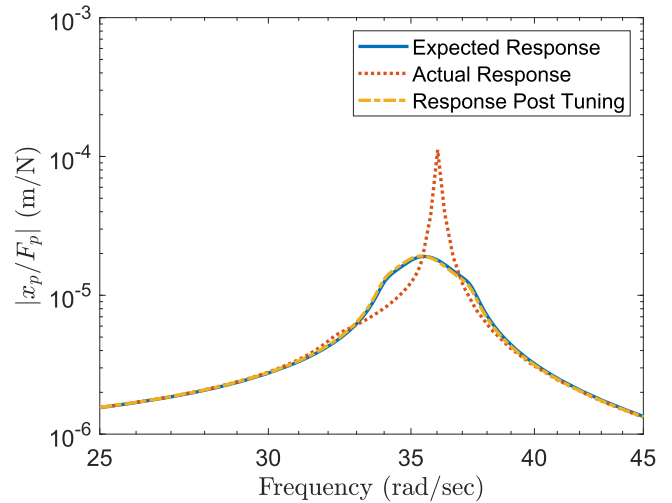


Figure 15. Frequency response function from the force applied F_p to the displacement x_p of a host structure attached to a PSOA. An error of -10% in the stiffness of the PSOA deteriorates the host structure’s response. However, the effect of error is eliminated after shunt tuning.

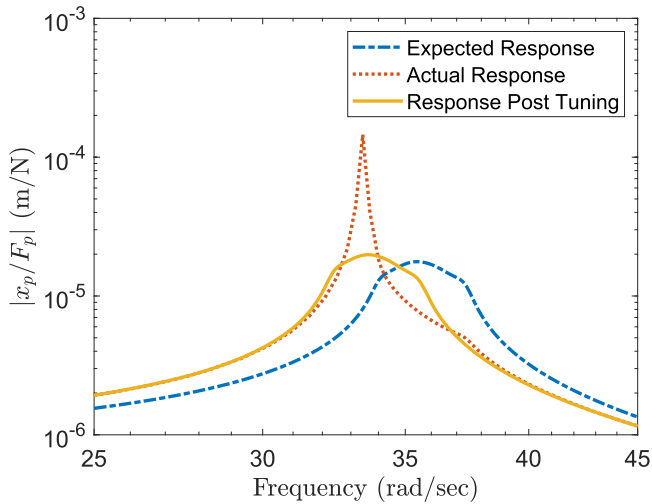


Figure 14. Frequency response function from the force applied F_p to the displacement x_p of a host structure. This plot shows that the effect of disorder on the host structure’s response can be mitigated by shunt tuning.

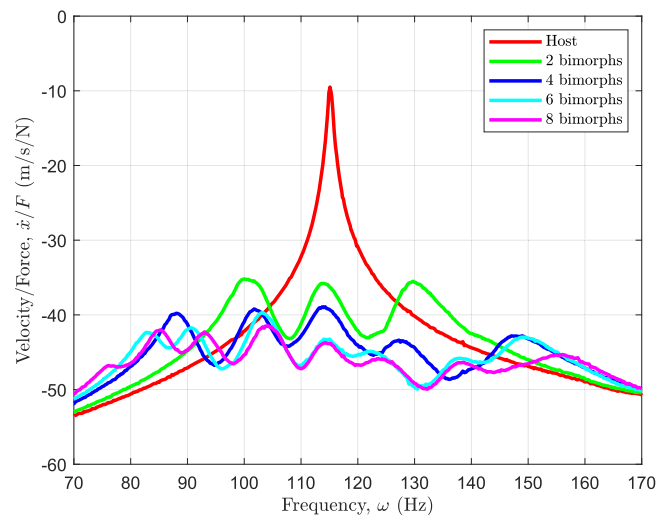


Figure 16. Experimental FRF from base acceleration to the tip velocity of the host structure with PSOAs.

8. Experimental results

As discussed in earlier sections, the first natural frequency of an aluminum beam was targeted for experimentally studying the performance of the PSOAs. Figure 16 shows the experimental frequency response function of the unmodified host (red) as well as the FRFs of the host with PSOAs. The structural details of the oscillators in the PSOA are tabulated in table 2. While the PSOA with two oscillators was able to achieve a 25 dB reduction, adding more oscillators resulted in a wider flattening of the bandwidth with at least 30 dB attenuation. The natural frequencies of the oscillators in the PSOA were selected such that their nondimensional frequencies would follow the selected distributions shown in figure 17. Revisiting equation (18), the nondimensional frequency is expressed as the ratio of nondimensional stiffness

and nondimensional mass, which also included mass of the subordinate oscillators. However, in figure 17, the non-dimensional frequency is defined for experimental results as the ratio of the damped natural frequency of the bimorphs to the damped natural frequency of the unmodified host. This definition is a good approximation of the theoretical non-dimensional frequency, as it is easier to estimate during experimentation.

Based on figure 16, it is evident that increasing the number of oscillators does not always have significant attenuation gains, especially considering the increase in the mass ratio at each step. However, the advantage of having more oscillators in PSOAs comes from an increase in its robustness. The robustness of vibration attenuation via PSOAs is evaluated through artificially changing the host’s

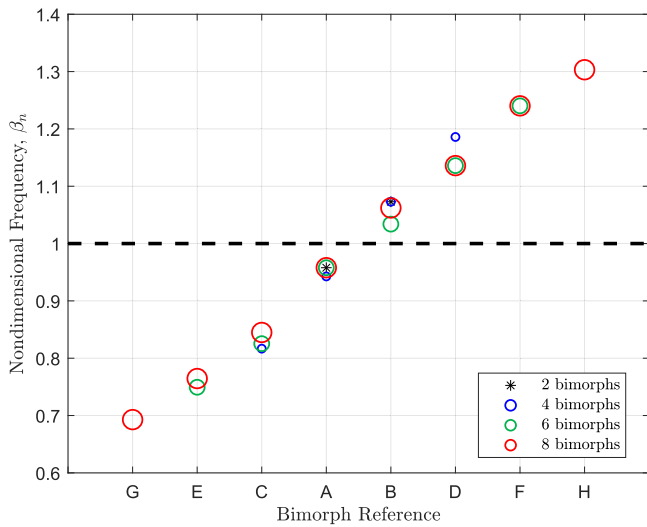


Figure 17. Nondimensional frequency distribution of the PSOA shown in figure 16. The oscillators in the PSOA are referenced out of order in the x -axis to maintain the symmetry and facilitate comparison of the nondimensional frequency distributions. The properties of all the oscillators can be referred from table 2 based on the oscillator reference.

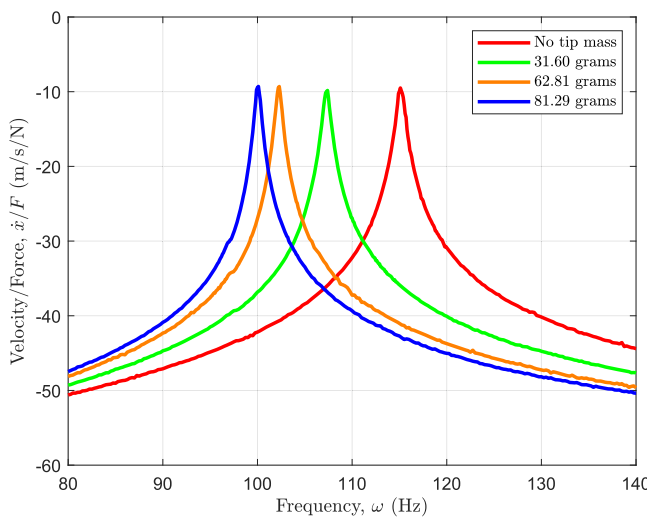


Figure 18. The variation of the host structure's FRFs with different tip masses. The tip masses mimic the degradation of host's properties over time.

natural frequency by adding tip mass. Figure 18 shows the change in the FRFs of the host structure with addition of tip masses. Consequently, the nondimensional frequency distribution of the PSOA is not tuned for the modified host. Even for a 15 Hz shift in natural frequency (or 13% change in nondimensional frequency), PSOA with four and eight oscillators were able to attenuate the resonant peak by about 25 dB, as seen in figure 19. It can also be seen that the PSOA with higher bandwidth (8 oscillator case) resulted in a flatter response; thereby displaying the robustness of PSOA. Additionally, in case of the PSOA with eight oscillators, shunt tuning was not necessary. On the other hand, shunt tuning improved the performance of the PSOA with four oscillators as shown in figure 20.

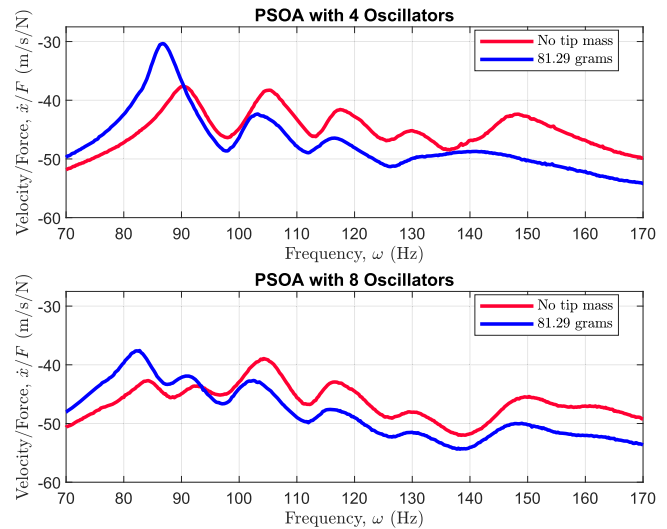


Figure 19. Experimental FRF from base acceleration to the tip velocity of the host structure with 4 and 8 oscillator PSOA.

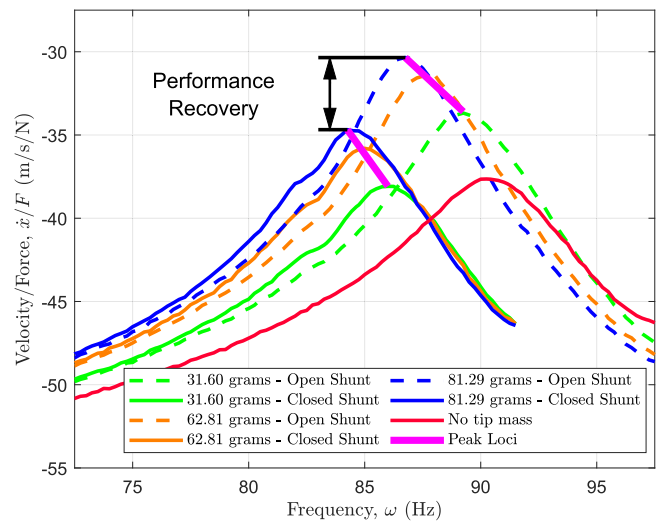


Figure 20. Four oscillator PSOA's performance recovery using shunt tuning.

In this figure, the red colored line (no tip mass) is the response of the original system with PSOA. With addition of tip masses to the host, the natural frequency of the host decreases and the magnitude increases at lower frequencies. As the PSOA are tuned with shunted circuits, the magnitude is partially recovered as pointed out in this figure. While the dashed line correspond to open circuits, the solid lines correspond to the PSOA with closed shunts. The difference in peak magnitudes gives a measure of the recovered performance. Loci of the peaks of open and closed circuit lines are also seen in figure 20. Extrapolation of these lines provides us with an idea of how the PSOA performs with changes or uncertainty in the dynamics of the host structure. It is important to notice that these lines are not parallel to each other. And this agrees with our intuition since we expect the performance recovery ability of the PSOA to decrease with increasing uncertainty. From a design perspective, we want the performance recovery ability of a PSOA to be as high as

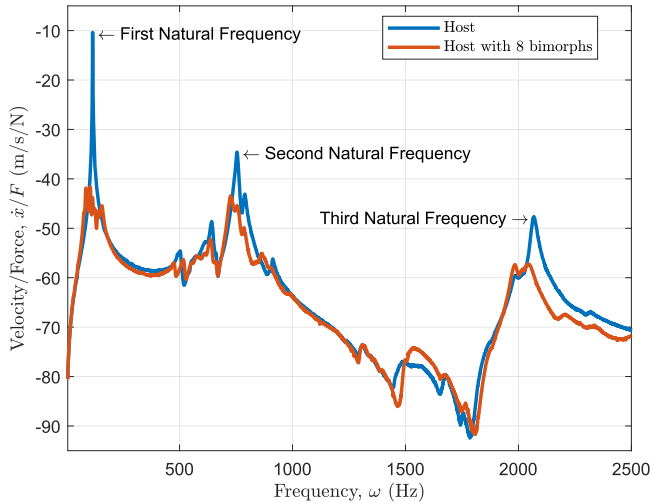


Figure 21. Broadband experimental FRF from base acceleration to the tip velocity of the host structure with 8 oscillator PSOA. The FRF shows that the modal spillover across a large frequency range is minimal. Additionally, the second and the third natural frequencies are also attenuated.

possible. This can be achieved by piezoelectric oscillator shunt tuning, which can be achieved by increasing the thickness of the bimorph's piezoelectric patches. Another approach would be to include negative capacitance [53, 83]. In situations where uncertainty can be higher, these factors should be considered, however these discussions are beyond the scope of the current paper and hence not addressed rigorously.

Figure 21 shows the FRFs of the host as well as the host with eight oscillators PSOA up to 2500 Hz. This figure is presented here to show that the amount of modal spillover outside the PSOA bandwidth. The performance deterioration is minimal in the displayed frequency range. Also, the second and third modes have been attenuated by about 10 dB. This can be attributed to the damping of and the absorption of high frequencies energies by the oscillators tuned to the first natural frequency.

9. Conclusions

This paper has shown that PSOAs can realize and improve on the benefits of ordinary SOAs and tunable DVAs. They can be used to achieve a flat response in the frequency domain and have the ability to address uncertainties in structural properties, at the expense of added complexity. The zero-nonzero block structure of the coupled PSOA and host system enables assignment of distributions to nondimensional electromechanical parameters. As shown both numerically and experimentally in this paper, the assignment of such distributions dramatically simplifies the design process and can eliminate the need for complex optimization methods. Furthermore, the idea of performance recovery is introduced to analyze the ability of PSOA's performance under uncertain structural parameters. It was shown experimentally that for limited levels of uncertainty, passive capacitance tuning could

recover the PSOA's flat frequency bandwidth after loss due to uncertainty. The tuning techniques described in this paper are limited to passive methods. As a topic of future study, it would be of interest to analyze how active circuits can also be implemented to tune the PSOAs adaptively.

Appendix A. Thermodynamic variational principles

Modeling of piezoelectric systems has been studied for decades, and various methods have been developed to model linear as well as nonlinear piezoelectric systems. Even though Newtonian techniques can be used to model piezoelectric systems [82], variational principles provide a systematic approach to derive consistent equations of motion when they are subject to nontrivial boundary conditions or couples to other electromechanical systems. In our problem the piezoelectric systems are attached to shunt circuits with resistors and capacitors. The variational principles for the piezoelectric system involve a modified form of classical Hamilton's principle [14, 82, 84–91]. The classical form of Hamilton's principle [82, 92] states that any trajectory in the mechanical configuration space must satisfy the variational identity

$$\delta \int_{t_0}^{t_1} (T - \mathcal{V}) dt + \int_{t_0}^{t_1} \delta W_{nc} dt = 0, \quad (\text{A.1})$$

where T is the kinetic energy of the system, \mathcal{V} is the potential energy of the system and δW_{nc} is the virtual work done by the nonconservative mechanical forces acting on the system. The variational formulations for piezoelectric systems use a modified form of equation (A.1) and are expressed in terms of electric enthalpy density \mathcal{H} or the internal energy density \mathcal{U} . The equivalence of the two variational principles is discussed using a simple example in [84].

A.1. \mathcal{H} variational principle

According to the \mathcal{H} variational principle, the actual motion of a piezoelectric system attached to a shunt circuit with a resistor, capacitor and current source in parallel must satisfy the variational identity

$$\delta \int_{t_0}^{t_1} (T - \mathcal{V}_{\mathcal{H}}) dt + \int_{t_0}^{t_1} \delta W_{\mathcal{H},nc} dt = 0 \quad (\text{A.2})$$

for all admissible variations of the actual electromechanical trajectory. In equation (A.2), T is the kinetic energy and $\mathcal{V}_{\mathcal{H}}$ is the electromechanical potential. It includes the potential energy of linearly elastic components and the contribution of the electrical enthalpy. The term δW_{nc} is the nonconservative virtual work done by the electromechanical loads on the system. The contribution of electric enthalpy to the electromechanical potential is expressed in the form

$$\mathcal{V}_{\mathcal{H}} := \int_{\Omega} \mathcal{H} d\Omega - \frac{1}{2} \sum_i C_i V_i^2. \quad (\text{A.3})$$

In equation (A.3), \mathcal{H} is the electric enthalpy density of the piezoelectric continua Ω , C_i is the capacitance of the i th capacitor in the shunt circuit, and V_i is the voltage across the

i th shunt circuit. The virtual work done by the non-conservative terms in a piezoelectric system attached to a shunt circuit has the form

$$\delta W_{\mathcal{H},nc} = \delta W_{nc} + \sum_j i_j \delta \lambda_j - \sum_k \frac{\dot{\lambda}_k}{R_k} \delta \lambda_k, \quad (\text{A.4})$$

where δW_{nc} is the virtual work term shown in equation (A.1) and λ_k is the flux linkage across the shunt circuit. The terms $\sum_j i_j \delta \lambda_j$ and $-\sum_k \frac{\dot{\lambda}_k}{R_k} \delta \lambda_k$ represent the virtual work contributions from the current source with current output i_k and the resistor with resistance R_k , respectively. The equations of motion obtained using this variational principle are expressed in terms of displacements and voltage/flux linkage as the generalized coordinates.

A.2. \mathcal{U} variational principle

The second variational principle used in this paper is the \mathcal{U} variational principle. It is expressed in terms of internal energy density of the system. According to this principle, the actual motion of a electromechanical system must satisfy the variational statement

$$\delta \int_{t_0}^{t_1} (T - \mathcal{V}_U) dt + \int_{t_0}^{t_1} \delta W_{\mathcal{U},nc} dt = 0 \quad (\text{A.5})$$

for all admissible variations of the actual electromechanical trajectory. In equation (A.5), T is the kinetic energy, \mathcal{V}_U is the electromechanical potential defined in terms of the internal energy density and $\delta W_{\mathcal{U},nc}$ is the nonconservative work done by the system. The expression for \mathcal{V}_U has the form

$$\mathcal{V}_U := \int_{\Omega} \mathcal{U} d\Omega + \frac{1}{2} \sum_i \frac{1}{C_i} Q_i^2, \quad (\text{A.6})$$

where \mathcal{U} is the internal energy density of the piezoelectric continua Ω , C_i is the capacitance of the i th capacitor in the shunt circuit, and Q_i is the charge flowing through the shunt circuit. The virtual work done $\delta W_{\mathcal{U},nc}$ is expressed in the form

$$\delta W_{\mathcal{U},nc} = \delta W_{nc} + \sum_j V_j \delta Q_j - \sum_k R_k \dot{Q}_k \delta Q_k, \quad (\text{A.7})$$

where δW_{nc} is the virtual work done shown in equation (A.1) and Q_k is the charge flowing through the shunt circuit. The terms $\sum_j V_j \delta Q_j$ and $-\sum_k R_k \dot{Q}_k \delta Q_k$ represent the virtual work contributions from the voltage source V_k and the resistor of resistance R_k respectively. The equations of motion derived using this variational principle are expressed in terms of the displacements and charge as the generalized coordinates.

Appendix B. Kinetic energy of a PSOA

The kinetic energy of a PSOA attached to a host structure is given in equation (4). Using separation of variables and Galerkin approximation, an approximation of the transverse displacement of each appendage is constructed as $w_i(x, t) = \sum_{j=1}^n \Psi_{ij}(x) \dot{W}_{ij}(t) = \Psi_i^T(x) \dot{W}_i(t)$. Substitution of the approximation into the expression for kinetic energy of the

distributed mass of each appendage results in

$$\begin{aligned} T_i &:= \frac{1}{2} \int_0^{L_i} \rho_i A_i ((\dot{x}_p - \dot{z}) + \dot{W}_i^T \Psi_i) \\ &\quad \times ((\dot{x}_p - \dot{z}) + \Psi_i^T \dot{W}_i) dx_i, \\ &= \frac{1}{2} \left[\underbrace{\int_0^{L_i} \rho_i A_i dx_i}_{\mathcal{M}_i} (\dot{x}_p - \dot{z})^2 \right. \\ &\quad + 2 \underbrace{\int_0^{L_i} \rho_i A_i \Psi_i^T dx_i}_{\mathcal{M}_{ip}^T} \dot{W}_i (\dot{x}_p - \dot{z}) \\ &\quad \left. + \dot{W}_i^T \underbrace{\int_0^{L_i} \rho_i A_i \Psi_i \Psi_i^T dx_i}_{\mathcal{M}_{ii}} \dot{W}_i \right], \\ &= \frac{1}{2} (\mathcal{M}_i (\dot{x}_p - \dot{z})^2 + 2 \mathcal{M}_{ip}^T \dot{W}_i (\dot{x}_p - \dot{z}) \\ &\quad + \dot{W}_i^T \mathcal{M}_{ii} \dot{W}_i). \end{aligned} \quad (\text{B.1})$$

Similarly, substitution of the approximation of the transverse displacement into the expression for kinetic energy of the tip mass of each appendage results in

$$\begin{aligned} T_i &= \frac{1}{2} m_i ((\dot{x}_p - \dot{z}) + \dot{W}_i^T \Psi_i(L_i)) \\ &\quad ((\dot{x}_p - \dot{z}) + \Psi_i^T(L_i) \dot{W}_i), \\ &= \frac{1}{2} (m_i (\dot{x}_p - \dot{z})^2 + 2 \underbrace{m_i \Psi_i^T(L_i)}_{\mathcal{M}_{ip}^T} \dot{W}_i (\dot{x}_p - \dot{z}) \\ &\quad + \dot{W}_i^T \underbrace{m_i \Psi_i(L_i) \Psi_i^T(L_i)}_{\mathcal{M}_{ii}} \dot{W}_i), \\ &= \frac{1}{2} (m_i (\dot{x}_p - \dot{z})^2 + 2 \mathcal{M}_{ip}^T \dot{W}_i (\dot{x}_p - \dot{z}) \\ &\quad + \dot{W}_i^T \mathcal{M}_{ii} \dot{W}_i). \end{aligned} \quad (\text{B.2})$$

Thus, the total kinetic energy of the system is expressed as

$$\begin{aligned} T &= \frac{1}{2} m_p (\dot{x}_p - \dot{z})^2 \\ &\quad + \sum_{i=1}^N \frac{1}{2} ((\mathcal{M}_i + m_i) (\dot{x}_p - \dot{z})^2 \\ &\quad + 2 (\mathcal{M}_{ip} + \mathcal{M}_{ip}^T)^T \dot{W}_i (\dot{x}_p - \dot{z}) \\ &\quad + \dot{W}_i^T (\mathcal{M}_{ii} + \mathcal{M}_{ii}) \dot{W}_i), \\ &= \frac{1}{2} m_p (\dot{x}_p - \dot{z})^2 + \sum_{i=1}^N \frac{1}{2} (M_i (\dot{x}_p - \dot{z})^2 \\ &\quad + 2 \mathcal{M}_{ip}^T \dot{W}_i (\dot{x}_p - \dot{z}) + \dot{W}_i^T \mathcal{M}_{ii} \dot{W}_i), \\ &= \frac{1}{2} M_{pp} (\dot{x}_p - \dot{z})^2 + \sum_{i=1}^N \frac{1}{2} (2 \mathcal{M}_{ip}^T \dot{W}_i (\dot{x}_p - \dot{z}) \\ &\quad + \dot{W}_i^T \mathcal{M}_{ii} \dot{W}_i), \end{aligned} \quad (\text{B.3})$$

where $M_{pp} := m_p + \sum_{i=1}^N M_i$.

Appendix C. Electromechanical potential of a PSOA

The total electromechanical potential of the system shown in figure 4 can be calculated using equation (A.3). However, as evident from the electric enthalpy density expression given in equation (6), the electric field E_i has to be calculated before proceeding further. The curl of the electric field across the bimorph beam is approximated as zero in the electrostatic approximation in linear piezoelectricity. Hence, electric field is expressed in the form $E_i(x_i, y_i, z_i) := -\frac{\delta\phi_i}{\delta z_i}$, where ϕ_i is the electric potential function. From the assumption of linear variation of potential across the piezoelectric patch, it follows that

$$E_i = \begin{cases} \frac{V_i}{t_{p,i}} & (x_i, y_i, z_i) \in \text{bottom patch,} \\ -\frac{V_i}{t_{p,i}} & (x_i, y_i, z_i) \in \text{top patch,} \\ 0 & \text{otherwise.} \end{cases} \quad (\text{C.1})$$

In equation (C.1), V_i and $t_{p,i}$ are the voltage across and thickness of the piezoelectric patch of the i th oscillator in the PSOA. The electromechanical potential can now be expressed using equation (A.3). It has the form

$$\begin{aligned} \mathcal{V}_{\mathcal{H}i} = & \frac{1}{2} \int_0^{L_i} \left(\int \int C_i^E z_i^2 dy_i dz_i \right) \left(\frac{\partial^2 w_i}{\partial x_i^2} \right)^2 dx_i \\ & + \int_0^{L_i} \left(\int \int e_i \kappa_i E_i dy_i dz_i \right) \frac{\partial^2 w_i}{\partial x_i^2} dx_i \\ & - \frac{1}{2} \int_0^{L_i} \left(\int \int \epsilon_i^S E_i^2 dy_i dz_i \right) dx_i - \frac{1}{2} C_i V_i^2. \end{aligned} \quad (\text{C.2})$$

Assuming the material stiffness to be uniform in the y and z direction, the term $\int \int C_i^E z_i^2 dy_i dz_i$ simplifies to $C_i^E I_i$ where I_i is the area moment of inertia of piezoelectric beam i . Defining the terms $\kappa_i := \kappa_{T_i} - \kappa_{B_i}$ with $\kappa_{T_i} := \int \int_{A_T} z_i dy_i dz_i$ for the top piezoelectric patch and $\kappa_{B_i} := \int \int_{A_B} z_i dy_i dz_i$ for the bottom piezoelectric patch simplifies the expression for the electromechanical potential to

$$\begin{aligned} \mathcal{V}_{\mathcal{H}i} = & \frac{1}{2} \int_0^{L_i} C_i^E I_i \left(\frac{\partial^2 w_i}{\partial x_i^2} \right)^2 dx_i \\ & - \int_0^{L_i} \frac{e_i \kappa_i}{t_{p,i}} \chi_{[a_i, b_i]} \frac{\partial^2 w_i}{\partial x_i^2} dx_i V_i(t) \\ & - \frac{1}{2} \frac{\epsilon_i^S 2A_{p,i}(b_i - a_i)}{t_{p,i}^2} V_i^2 - \frac{1}{2} C_i V_i^2. \end{aligned} \quad (\text{C.3})$$

As shown in figure 5, a_i and b_i in the above equation are the left and right piezoelectric patch coordinates, respectively. The piezoelectric cross sectional area is defined as $A_{p,i} := t_{p,i} \cdot \mathcal{W}_i$, where $t_{p,i}$ and \mathcal{W}_i are the thickness and width of the piezoelectric patch, respectively. The function $\chi_{[a_i, b_i]}$ in the equation (C.3) is called the characteristic function and is defined as

$$\chi_{[a_i, b_i]}(x) := \begin{cases} 1, & \text{if } x \in [a_i, b_i], \\ 0, & \text{otherwise.} \end{cases} \quad (\text{C.4})$$

Substituting the Galerkin approximation for transverse displacement of each substructure $w_i = \sum_{i=1}^n \Psi_i(x) W_i(t) = \Psi_i(x) \mathbf{W}_i(t)$ into the above expression generates the expression

$$\mathcal{V}_{\mathcal{H}i} = \frac{1}{2} \mathbf{W}_i^T \mathbf{K}_{ii} \mathbf{W}_i - \mathbf{B}_i^T \mathbf{W}_i V_i - \frac{1}{2} D_i V_i^2 - \frac{1}{2} C_i V_i^2, \quad (\text{C.5})$$

where

$$\begin{aligned} \mathbf{K}_{ii} & := \int_0^{L_i} C_i^E I_i \Psi_i'' \Psi_i''^T dx_i, \\ \mathbf{B}_i^T & := \int_0^{L_i} \frac{\kappa_i e_i}{t_{p,i}} \chi_{[a_i, b_i]} \Psi_i''^T dx_i, \\ D_i & := \frac{\epsilon_i^S 2A_{p,i}(b_i - a_i)}{t_{p,i}^2}. \end{aligned} \quad (\text{C.6})$$

Appendix D. Host structure with a PSOA model

In this section, the steps involved in deriving the equation of motion of a PSOA attached to a host structure are given. Further simplification of the above expressions in equations (4), (7) and (9) is achieved by introducing the block vectors and matrices

$$\begin{aligned} \mathbb{W} & := \{\mathbf{W}_1 \dots \mathbf{W}_N\}^T, \quad \mathbb{V} := \{V_1 \dots V_N\}^T, \\ \mathbf{i} & := \{\mathbf{i}_1 \dots \mathbf{i}_N\}^T, \quad \mathbf{\Lambda} := \{\lambda_1 \dots \lambda_N\}^T, \\ \mathbb{M}_p & := \{\mathbf{M}_1 \dots \mathbf{M}_N\}^T, \end{aligned} \quad (\text{D.1})$$

$$\begin{aligned} \mathbb{M} & := \text{diag}(\mathbf{M}_{11}, \mathbf{M}_{22}, \dots, \mathbf{M}_{NN}), \\ \mathbb{B} & := \text{diag}(\mathbf{B}_1, \mathbf{B}_2, \dots, \mathbf{B}_N), \\ \mathbb{K} & := \text{diag}(\mathbf{K}_{11}, \mathbf{K}_{22}, \dots, \mathbf{K}_{NN}), \\ \mathbb{D} & := \text{diag}(D_1, D_2, \dots, D_N), \\ \mathbf{\zeta} & := \text{diag}\left(\frac{1}{R_1}, \frac{1}{R_2}, \dots, \frac{1}{R_N}\right) \\ \mathbf{C} & := \text{diag}(C_1, C_2, \dots, C_N). \end{aligned} \quad (\text{D.2})$$

The final equation for kinetic energy, electromechanical potential energy and virtual work done then has the form

$$\begin{aligned} T & = \frac{1}{2} (\mathbf{M}_{pp} \dot{x}_p - \dot{\mathfrak{z}})^2 \\ & + 2(\dot{x}_p - \dot{\mathfrak{z}}) \mathbf{M}_p^T \dot{\mathbb{W}} + \dot{\mathbb{W}}^T \mathbf{M} \mathbb{W}, \end{aligned} \quad (\text{D.3})$$

$$\begin{aligned} \mathcal{V}_{\mathcal{H}} & = \frac{1}{2} (\mathbf{K}_p x_p^2 + \mathbb{W}^T \mathbf{K} \mathbb{W} \\ & - 2\mathbb{V}^T \mathbf{B}^T \mathbb{W} - \mathbb{V}^T \mathbf{D} \mathbb{V} - \mathbb{V}^T \mathbf{C} \mathbb{V}), \end{aligned} \quad (\text{D.4})$$

$$\begin{aligned} \delta W_{nc} & = F_p \delta(x_p - \mathfrak{z}) + \mathbf{i}^T \delta \mathbf{\Lambda} - \mathbf{\Lambda}^T \mathbf{\zeta} \delta \mathbf{\Lambda} - \delta \mathbf{q}^T \mathbf{C} \dot{\mathbf{q}}, \\ & = F_p \delta(x_p - \mathfrak{z}) + \mathbf{i}^T \delta \mathbf{\Lambda} - \mathbf{\Lambda}^T \mathbf{\zeta} \delta \mathbf{\Lambda} \\ & - \delta x_p C_p \dot{x}_p - \delta \mathbb{W}^T \mathbf{C} \dot{\mathbb{W}}. \end{aligned} \quad (\text{D.5})$$

The \mathcal{H} variational principle can now be applied to derive the equations of motion of host structure attached to the PSOA. Recall that the equations of motion must satisfy the \mathcal{H} variational principle we discussed in Subsection appendix A.1.

After substituting T , $\mathcal{V}_{\mathcal{H}}$ and δW_{nc} into equation (A.2), the variational statement yields

$$\begin{aligned} & \int_{t_0}^{t_1} \{M_{pp}(\dot{x}_p - \dot{\mathfrak{z}})\delta(\dot{x}_p - \dot{\mathfrak{z}}) + \mathbb{M}_p^T \dot{\mathbb{W}}\delta(\dot{x}_p - \dot{\mathfrak{z}}) \\ & + (\dot{x}_p - \dot{\mathfrak{z}})\mathbb{M}_p^T \delta \dot{\mathbb{W}} + \delta \dot{\mathbb{W}}^T \mathbb{M} \dot{\mathbb{W}}\} dt \\ & - \int_{t_0}^{t_1} \{\delta \mathbb{W}^T \mathbb{K} \mathbb{W} - \delta \mathbb{V}^T \mathbb{B}^T \mathbb{W} - \delta \mathbb{W}^T \mathbb{B} \mathbb{V} \\ & - \delta \mathbb{V}^T \mathbb{D} \mathbb{V} - \delta \mathbb{V}^T \mathbb{C} \mathbb{V} + K_p x_p \delta x_p\} dt \\ & + \int_{t_0}^{t_1} \{F_p \delta(x_p - \mathfrak{z}) - \dot{\Lambda}^T \zeta \delta \Lambda - \delta \mathbb{W}^T \mathbb{C} \dot{\mathbb{W}} \\ & - \delta x_p C_p \dot{x}_p + \dot{\mathfrak{z}}^T \delta \Lambda\} dt = 0. \end{aligned} \quad (\text{D.6})$$

The base motion \mathfrak{z} is a prescribed input for this system. Hence, we have $\delta(x_p - \mathfrak{z}) = \delta x_p$. Rearranging the terms in the above expression and integration by parts results in the variational expression

$$\begin{aligned} & \int_{t_0}^{t_1} \{\delta x_p (-M_{pp}(\ddot{x}_p - \ddot{\mathfrak{z}}) - \mathbb{M}_p \ddot{\mathbb{W}} - C_p \dot{x}_p - K_p x_p + F_p) \\ & + \delta \mathbb{W}^T (-\mathbb{M}_p(\ddot{x}_p - \ddot{\mathfrak{z}}) - \mathbb{M} \ddot{\mathbb{W}} - \mathbb{C} \dot{\mathbb{W}} - \mathbb{K} \mathbb{W} + \mathbb{B} \mathbb{V}) \\ & + \delta \Lambda^T (-\mathbb{B}^T \dot{\mathbb{W}} - \mathbb{D} \dot{\mathbb{V}} - \zeta \dot{\Lambda} + \dot{\mathfrak{z}} - \mathbb{C} \dot{\mathbb{V}})\} dt \\ & + \text{variational BCs} = 0, \end{aligned} \quad (\text{D.7})$$

which must hold for all admissible variations δx_p , $\delta \mathbb{W}$ and $\delta \Lambda$. It is shown in [82] that the variational boundary conditions above are zero. Finally, the equations of motion of the system under consideration are

$$\begin{aligned} & \begin{bmatrix} \mathbb{M} & \mathbb{M}_p \\ \mathbb{M}_p^T & M_{pp} \end{bmatrix} \begin{Bmatrix} \ddot{\mathbb{W}} \\ \ddot{x}_p - \ddot{\mathfrak{z}} \end{Bmatrix} + \begin{bmatrix} \mathbb{C} & \mathbf{0} \\ \mathbf{0}^T & C_p \end{bmatrix} \begin{Bmatrix} \dot{\mathbb{W}} \\ \dot{x}_p \end{Bmatrix} \\ & + \begin{bmatrix} \mathbb{K} & \mathbf{0} \\ \mathbf{0}^T & K_p \end{bmatrix} \begin{Bmatrix} \mathbb{W} \\ x_p \end{Bmatrix} - \begin{bmatrix} \mathbb{B} \\ \mathbf{0} \end{bmatrix} \mathbb{V} = \begin{Bmatrix} \mathbf{0} \\ F_p \end{Bmatrix}, \end{aligned} \quad (\text{D.8})$$

or

$$\begin{aligned} & \begin{bmatrix} \mathbb{M} & \mathbb{M}_p \\ \mathbb{M}_p^T & M_{pp} \end{bmatrix} \begin{Bmatrix} \ddot{\mathbb{W}} \\ \ddot{x}_p \end{Bmatrix} + \begin{bmatrix} \mathbb{C} & \mathbf{0} \\ \mathbf{0}^T & C_p \end{bmatrix} \begin{Bmatrix} \dot{\mathbb{W}} \\ \dot{x}_p \end{Bmatrix} \\ & + \begin{bmatrix} \mathbb{K} & \mathbf{0} \\ \mathbf{0}^T & K_p \end{bmatrix} \begin{Bmatrix} \mathbb{W} \\ x_p \end{Bmatrix} - \begin{bmatrix} \mathbb{B} \\ \mathbf{0} \end{bmatrix} \mathbb{V} = \begin{Bmatrix} \mathbf{0} \\ \hat{F}_p \end{Bmatrix}, \end{aligned} \quad (\text{D.9})$$

where $\hat{F}_p = F_p + M_{pp} \ddot{\mathfrak{z}}$ and

$$\mathbb{B}^T \dot{\mathbb{W}} + \mathbb{D} \dot{\mathbb{V}} + \zeta \dot{\Lambda} - \dot{\mathfrak{z}} + \mathbb{C} \dot{\mathbb{V}} = \mathbf{0}. \quad (\text{D.10})$$

Appendix E. Closed form expression for frequency response function

The current section is focused on deriving the frequency response function from the force input F_p to the displacement x_p of the primary structure. The transfer function from the force input to the displacement of a host structure attached to a PSOA with capacitive shunt is given by equation (15). Evaluating this transfer function along the imaginary axis can

find the required FRF. However, we seek a FRF that is similar in form to the expression in equation (1) [11]. To achieve this, we introduce a change of variables

$$\begin{Bmatrix} \mathbb{W} \\ x_p \end{Bmatrix} = \underbrace{\begin{bmatrix} I & -\alpha \\ \mathbf{0}^T & 1 \end{bmatrix}}_{\Gamma} \begin{Bmatrix} \mathbb{X}_s \\ x_p \end{Bmatrix} \quad (\text{E.1})$$

in equation (15) and premultiply the same equation by Γ^T . This change in variables removes the mass coupling in the transfer function. In equation (E.1), $\alpha := \mathbb{M}^{-1} \mathbb{M}_p$, and \mathbb{X}_s is analogous to the absolute displacement of the piezoelectric beam. After the change in variables in equation (15), we have

$$\begin{bmatrix} \mathbb{M} s^2 + \mathbb{C} s + \hat{\mathbb{K}} & -(\mathbb{C} s + \hat{\mathbb{K}}) \alpha \\ -((\mathbb{C} s + \hat{\mathbb{K}}) \alpha)^T & \bar{M}_{pp} s^2 + \bar{C}_p s + \bar{K}_p \end{bmatrix} \begin{Bmatrix} \mathbb{X}_s \\ x_p \end{Bmatrix} = \begin{Bmatrix} \mathbf{0} \\ f_p(s) \end{Bmatrix}, \quad (\text{E.2})$$

where the terms \bar{M}_{pp} , \bar{C}_p , \bar{K}_p have the definitions $\bar{M}_{pp} := (M_{pp} - \alpha^T \mathbb{M}_p)$, $\bar{C}_p := (C_p + \alpha^T \mathbb{C} \alpha)$, $\bar{K}_p := (K_p + \alpha^T \mathbb{K} \alpha)$. From equation (E.2), we have the relations

$$\mathbb{X}_s = (\mathbb{M} s^2 + \mathbb{C} s + \hat{\mathbb{K}})^{-1} (\mathbb{C} s + \hat{\mathbb{K}}) \alpha x_p, \quad (\text{E.3})$$

$$-((\mathbb{C} s + \hat{\mathbb{K}}) \alpha)^T \mathbb{X}_s + [\bar{M}_{pp} s^2 + \bar{C}_p s + \bar{K}_p] x_p = f_p(s). \quad (\text{E.4})$$

Equation (E.3) represents the relation between the motion of the primary mass and motion of the substructures. The transfer function from the applied force to the displacement of the primary structure is obtained by substituting equation (E.3) into equation (E.4). As is well known, using modal or Fourier shape functions yields matrices and submatrices \mathbb{M} , \mathbb{K} , \mathbb{C} , \mathbb{B} and \mathbb{D} that are diagonal. As defined in the earlier sections, the elements of \mathbb{M} , \mathbb{M}_p , \mathbb{K} , \mathbb{C} and \mathbb{B} are M_{nn} , M_{np} , K_{nn} , C_{nn} and B_n , respectively. With single mode approximation these elements reduce to scalars which are denoted by M_{nn} , M_{np} , K_{nn} , C_{nn} and B_n , respectively. With these assumptions, it is easier to derive the transfer function which is given by

$$\begin{aligned} \frac{x_p(s)}{f_p(s)} &= \left\{ M_{pp} s^2 + C_p s + K_p \right. \\ &+ \sum_{n=1}^N \left[-\alpha_n M_{np} s^2 + \alpha_n^2 C_{nn} s \right. \\ &\left. \left. + \alpha_n^2 \hat{K}_{nn} - \frac{(C_{nn} \alpha_n s + \hat{K}_{nn} \alpha_n)^2}{M_{nn} s^2 + C_{nn} s + \hat{K}_{nn}} \right] \right\}^{-1}. \end{aligned} \quad (\text{E.5})$$

The transfer function in the case of multi-mode approximation will look very similar to equation (E.5) and can be derived using the same procedure shown above. Substituting $s = i\omega$ into equation (E.5) results in an expression for the frequency response function

$$\frac{x_p(i\omega)}{f_p(i\omega)} = \left\{ -M_{pp}\omega^2 + iC_p\omega + K_p + \sum_{n=1}^N \left[\alpha_n M_{np}\omega^2 + \alpha_n^2 \left[iC_{nn}\omega + \hat{K}_{nn} - \frac{(iC_{nn}\omega + \hat{K}_{nn})^2}{-M_{nn}\omega^2 + iC_{nn}\omega + \hat{K}_{nn}} \right] \right] \right\}^{-1} \quad (\text{E.6})$$

ORCID iDs

Sai Tej Paruchuri  <https://orcid.org/0000-0003-2372-3888>

References

- [1] Inman D J 2001 Engineering vibration *Vibration Fundamentals and Practice* (Upper Saddle River, NJ: Pearson Education)
- [2] Kitis L, Wang B P P and Pilkey W D D 1983 Vibration reduction over a frequency range *J. Sound Vib.* **89** 559–69
- [3] Villaverde R 1985 Reduction seismic response with heavily-damped vibration absorbers *Earthq. Eng. Struct. Dyn.* **13** 33–42
- [4] Thompson A G 1981 Optimum tuning and damping of a dynamic vibration absorber applied to a force excited and damped primary system *J. Sound Vib.* **77** 403–15
- [5] Randall S E III, Halsted D M and Taylor D L 1981 Optimum vibration absorbers for linear damped systems *J. Mech. Des.* **103** 908–13
- [6] Pennestrì E 1998 An application of chebyshev's minmax criterion to the optimal design of a damped dynamic vibration absorber *J. Sound Vib.* **217** 757–65
- [7] Strasberg M and Feit D 1996 Vibration damping of large structures induced by attached small resonant structures *J. Acoust. Soc. Am.* **99** 335–44
- [8] Akay A, Xu Z, Carcaterra A and Koc I M 2005 Experiments on vibration absorption using energy sinks *J. Acoust. Soc. Am.* **118** 3043
- [9] Zuo L and Nayfeh S A 2005 Optimization of the individual stiffness and damping parameters in multiple-tuned-mass-damper systems *J. Vib. Acoust.* **127** 77
- [10] Carcaterra A, Akay A and Bernardini C 2012 Trapping of vibration energy into a set of resonators: theory and application to aerospace structures *Mech. Syst. Signal Process.* **26** 1–14
- [11] Vignola J F, Judge J A and Kurdila A J 2009 Shaping of a system's frequency response using an array of subordinate oscillators *J. Acoust. Soc. Am.* **126** 129–39
- [12] Banks H T, Smith R C and Wang Y 1996 *Smart Material Structures: Modeling, Estimation, and Control* (Chichester: Wiley) 1940
- [13] Craig R R and Kurdila A J 2006 *Fundamentals of Structural Dynamics* (New York: Wiley)
- [14] Tiersten H F 1969 *Linear Piezoelectric Plate Vibrations* (Boston, MA: Springer)
- [15] Vignola J, Glean A, Judge J and Ryan T 2013 Optimal apparent damping as a function of the bandwidth of an array of vibration absorbers *J. Acoust. Soc. Am.* **134** 1067–70
- [16] Vignola J, Judge J, Sterling J, Ryan T, Kurdila A, Paruchuri S T and Glean A 2016 On the use of shunted piezo actuators for mitigation of distribution errors in resonator arrays *Proc. 22nd Int. Congress on Acoustics* (<http://www.ica2016.org.ar/ica2016proceedings/ica2016/ICA2016-0798.pdf>)
- [17] Maidanik G 2001 Induced damping by a nearly continuous distribution of nearly undamped oscillators: linear analysis *J. Sound Vib.* **240** 717–31
- [18] Nagem R 1997 Vibration damping by a continuous distribution of undamped oscillators *J. Sound Vib.* **207** 429–34
- [19] Hagood N W, Chung W H and Von Flotow A 1990 Modelling of piezoelectric actuator dynamics for active structural control *J. Intell. Mater. Syst. Struct.* **1** 327–54
- [20] Fleming A J, Behrens S and Moheimani S O R 2000 Synthetic impedance for implementation of piezoelectric shunt-damping circuits *Electron. Lett.* **36** 1525–6
- [21] Tylikowski A 2000 Distributed piezoelectric vibration absorbers *ZAMM—J. Appl. Math. Mech./Z. Angew. Math. Mech.* **80** 305–6
- [22] Tylikowski A 2001 Control of circular plate vibrations via piezoelectric actuators shunted with a capacitive circuit *Thin-Walled Struct.* **39** 83–94
- [23] Granier J J, Haundhausen R J and Gaytan G E 2001-01-01 Passive Modal Damping with Piezoelectric Shunts *20th International Modal Analysis Conference (Los Angeles, CA, February 4–7, 2002)* (<https://permalink.lanl.gov/object/tr?what=info:lanl-repo/lareport/LA-UR-01-5620>)
- [24] Al-Ahmad M, Rolland N and Rolland P 2006 Piezoelectric-based tunable microstrip shunt resonator *2006 Asia-Pacific Microwave Conf.* pp 653–6
- [25] Casadei F, Dozio L, Ruzzene M and Cunefare K A 2010 Periodic shunted arrays for the control of noise radiation in an enclosure *J. Sound Vib.* **329** 3632–46
- [26] Airoidi L and Ruzzene M 2011 Wave propagation control in beams through periodic multi-branch shunts *J. Intell. Mater. Syst. Struct.* **22** 1567–79
- [27] Airoidi L and Ruzzene M 2011 Design of tunable acoustic metamaterials through periodic arrays of resonant shunted piezos *New J. Phys.* **13** 113010
- [28] Wen G W, Chen S and Jihong W 2011 Low-frequency locally resonant band gaps induced by arrays of resonant shunts with Antoniou's circuit: experimental investigation on beams *Smart Mater. Struct.* **20** 15026
- [29] Beck B S, Cunefare K A, Collet M and Ruzzene M 2011 Active vibration control of a stiffened panel through application of negative capacitance shunts *Proc. SPIE 7977, Active and Passive Smart Structures and Integrated Systems 2011, 79770C* 27 April 2011) (<https://doi.org/10.1117/12.880418>)
- [30] Thomas O, Ducarne J and Deü J-F 2012 Performance of piezoelectric shunts for vibration reduction *Smart Mater. Struct.* **21** 15008
- [31] Lu Y and Tang J 2012 Electromechanical tailoring of structure with periodic piezoelectric circuitry *J. Sound Vib.* **331** 3371–85
- [32] Casadei F, Beck B S, Cunefare K A and Ruzzene M 2012 Vibration control of plates through hybrid configurations of periodic piezoelectric shunts *J. Intell. Mater. Syst. Struct.* **23** 1169–77
- [33] Chen S, Wang G, Wen J and Wen X 2013 Wave propagation and attenuation in plates with periodic arrays of shunted piezo-patches *J. Sound Vib.* **332** 1520–32
- [34] Casadei F and Bertoldi K 2014 Wave propagation in beams with periodic arrays of airfoil-shaped resonating units *J. Sound Vib.* **333** 6532–47
- [35] Guo K M and Jiang J 2014 Independent modal resonant shunt for multimode vibration control of a truss-cored sandwich panel *Int. J. Dyn. Control* **2** 326–34
- [36] Lossouarn B, Deü J-F, Aucejo M and Cunefare K A 2016 Multimodal vibration damping of a plate by piezoelectric coupling to its analogous electrical network *Smart Mater. Struct.* **25** 115042

- [37] Larbi W, Deü J-F and Ohayon R 2016 Finite element reduced order model for noise and vibration reduction of double sandwich panels using shunted piezoelectric patches *Appl. Acoust.* **108** 40–9
- [38] Lossouarn B, Aucejo M, Deü J-F and Multon B 2017 Design of inductors with high inductance values for resonant piezoelectric damping *Sensors Actuators A* **259** 68–76
- [39] Clark W W 1999 Semi-active vibration control with piezoelectric materials as variable-stiffness actuators *Proc. SPIE 3672, Smart Structures and Materials 1999: Passive Damping and Isolation* 2 June 1999 (<https://doi.org/10.1117/12.349775>)
- [40] Richard C, Guyomar D, Audigier D and Ching G 1999 Semi-passive damping using continuous switching of a piezoelectric device *Proc. SPIE 3672, Smart Structures and Materials 1999: Passive Damping and Isolation* 2 June 1999 (<https://doi.org/10.1117/12.349773>)
- [41] Clark W W 2000 Vibration control with state-switched piezoelectric materials *J. Intell. Mater. Syst. Struct.* **11** 263–71
- [42] Cunefare K A, de Rosa S, Sadegh N and Larson G 2000 State-switched absorber for semi-active structural control *J. Intell. Mater. Syst. Struct.* **11** 300–10
- [43] Morgan R A and Wang K-W 2001 Multifrequency piezoelectric vibration absorber for variable frequency harmonic excitations *Proc. SPIE 4331, Smart Structures and Materials 2001: Damping and Isolation* 2 July 2001 (<https://doi.org/10.1117/12.432697>)
- [44] Holdhusen M, Cunefare K and Larson G D 2001 Role of damping in state-switched absorber for vibration control *Proc. SPIE 4326, Smart Structures and Materials 2001: Modeling, Signal Processing, and Control in Smart Structures* 21 August 2001 (<https://doi.org/10.1117/12.436477>)
- [45] Cunefare K A 2002 State-switched absorber for vibration control of point-excited beams *J. Intell. Mater. Syst. Struct.* **13** 97–105
- [46] Holdhusen M H and Cunefare K A 2004 Optimization of a state-switched absorber applied to a continuous vibrating system *Proc. SPIE 5386, Smart Structures and Materials 2004: Damping and Isolation* 29 July 2004 (<https://doi.org/10.1117/12.539876>)
- [47] Badel A, Sebald G, Guyomar D, Lallart M, Lefeuvre E, Richard C and Qiu J 2006 Piezoelectric vibration control by synchronized switching on adaptive voltage sources: towards wideband semi-active damping *J. Acoust. Soc. Am.* **119** 2815–25
- [48] Niederberger D and Morari M 2006 An autonomous shunt circuit for vibration damping *Smart Mater. Struct.* **15** 359–64
- [49] Ji H, Qiu J, Badel A and Zhu K 2008 Semi-active vibration control of a composite beam using an adaptive SSDV approach *J. Intell. Mater. Syst. Struct.* **20** 401–12
- [50] Qiu J, Ji H and Zhu K 2009 Semi-active vibration control using piezoelectric actuators in smart structures *Front. Mech. Eng. Chin.* **4** 242–51
- [51] Ji H 2010 *Semi-Active Vibration Control Based on Switched Piezoelectric Transducers* (Rijeka: IntechOpen) Chapter 10 (<https://doi.org/10.5772/10146>)
- [52] Cheng J, Ji H, Qiu J and Takagi T 2011 Semi-active vibration suppression by a novel synchronized switch circuit with negative capacitance *Int. J. Appl. Electromagn. Mech.* **37** 291–308
- [53] Mokrani B, Rodrigues G, Ioan B, Bastaitis R and Preumont A 2012 Synchronized switch damping on inductor and negative capacitance *J. Intell. Mater. Syst. Struct.* **23** 2065–75
- [54] Davis C L, Lesieutre G A and Dosch J J 1997 Tunable electrically shunted piezoceramic vibration absorber *Proc. SPIE 3045, Smart Structures and Materials 1997: Passive Damping and Isolation* 9 May 1997 (<https://doi.org/10.1117/12.274188>)
- [55] Davis C L and Lesieutre G A 1998 Actively tuned solid state piezoelectric vibration absorber *Proc. SPIE 3327, Smart Structures and Materials 1998: Passive Damping and Isolation* 16 June 1998 (<https://doi.org/10.1117/12.310681>)
- [56] Davis C L and Lesieutre G A 2000 An actively tuned solid-state vibration absorber using capacitive shunting of piezoelectric stiffness *J. Sound Vib.* **232** 601–17
- [57] Holdhusen M and Cunefare K A 2003 Optimization of location and tuning of a state-switched absorber for controlling beam vibration *Proc. SPIE 5049, Smart Structures and Materials 2003: Modeling, Signal Processing, and Control* 1 August 2003 (<https://doi.org/10.1117/12.484014>)
- [58] Ducarne J, Thomas O and Deü J-F 2012 Placement and dimension optimization of shunted piezoelectric patches for vibration reduction *J. Sound Vib.* **331** 3286–303
- [59] da Silva L P, Larbi W and Deü J-F 2014 Topology optimization of shunted piezoelectric elements for structural vibration reduction *J. Intell. Mater. Syst. Struct.* **26** 1219–35
- [60] Kong N, Ha D S, Erturk A and Inman D J 2010 Resistive impedance matching circuit for piezoelectric energy harvesting *J. Intell. Mater. Syst. Struct.* **21** 1293–302
- [61] Yang Y and Tang L 2009 Equivalent circuit modeling of piezoelectric energy harvesters *J. Intell. Mater. Syst. Struct.* **20** 2223–35
- [62] Carnegie D 2007 Frequency tuning concepts for piezoelectric cantilever beams *MS Thesis University of Pittsburgh* (<https://core.ac.uk/download/pdf/12207688.pdf>)
- [63] Wang X and Lin L 2013 Dimensionless optimization of piezoelectric vibration energy harvesters with different interface circuits *Smart Mater. Struct.* **22** 085011
- [64] Motter D, Dias F A and Silva S 2006 Vibration energy harvesting using piezoelectric transducer and non-controlled rectifiers circuits *J. Braz. Soc. Mech. Sci. & Eng.* **34** pp. 378–385
- [65] Badel A, Guyomar D, Lefeuvre E and Richard C 2005 Efficiency enhancement of a piezoelectric energy harvesting device in pulsed operation by synchronous charge inversion *J. Intell. Mater. Syst. Struct.* **16** 889–901
- [66] Adhikari S, Friswell M I and Inman D J 2009 Piezoelectric energy harvesting from broadband random vibrations *Smart Mater. Struct.* **18** 115005
- [67] Kim W K 2012 Design and analysis of switching circuits for energy harvesting in piezostructures *PhD Thesis Virginia Polytechnic Institute and State University*
- [68] Harn R L 2012 The study and development of distributed devices for concurrent vibration attenuation and energy harvesting *PhD Thesis Virginia Polytechnic Institute and State University*
- [69] Chen Y-Y, Vasic D, Liu Y-P and Costa F 2012 Study of a piezoelectric switching circuit for energy harvesting with bistable broadband technique by work-cycle analysis *J. Intell. Mater. Syst. Struct.* **24** 180–93
- [70] Ottman G K, Hofmann H F and Lesieutre G A 2003 Optimized piezoelectric energy harvesting circuit using step-down converter in discontinuous conduction mode *IEEE Trans. Power Electron.* **18** 696–703
- [71] Chen S-B, Wen J-H, Wang G, Han X-Y and Wen X-S 2011 Locally resonant gaps of phononic beams induced by periodic arrays of resonant shunts *Chin. Phys. Lett.* **28** 94301
- [72] Wang J-W, Wang G, Chen S-B and Wen J-H 2012 Broadband attenuation in phononic beams induced by periodic arrays of feedback shunted piezoelectric patches *Chin. Phys. Lett.* **29** 64302

- [73] Chen S-B, Wen J-H, Wang G and Wen X-S 2013 Tunable band gaps in acoustic metamaterials with periodic arrays of resonant shunted piezos *Chin. Phys. B* **22** 74301
- [74] Huang T L, Ichchou M N, Bareille O A, Collet M and Ouisse M 2013 Multi-modal wave propagation in smart structures with shunted piezoelectric patches *Comput. Mech.* **52** 721–39
- [75] Zhang H, Wen J-H, Chen S-B, Wang G and Wen X-S 2015 Flexural wave band-gaps in phononic metamaterial beam with hybrid shunting circuits *Chin. Phys. B* **24** 36201
- [76] Lian Z, Jiang S, Hu H, Dai L, Chen X and Jiang W 2016 An enhanced plane wave expansion method to solve piezoelectric phononic crystal with resonant shunting circuits *Shock Vib.* **2016** 4015363
- [77] Yi K, Collet M, Ichchou M and Li L 2016 Flexural waves focusing through shunted piezoelectric patches *Smart Mater. Struct.* **25** 75007
- [78] Sugino C, Leadenham S, Ruzzene M and Erturk A 2017 An investigation of electroelastic bandgap formation in locally resonant piezoelectric metastructures *Smart Mater. Struct.* **26** 55029
- [79] Jiang S, Dai L, Chen H, Hu H, Jiang W and Chen X 2017 Folding beam-type piezoelectric phononic crystal with low-frequency and broad band gap *Appl. Math. Mech.* **38** 411–22
- [80] Sugino C, Ruzzene M and Erturk A 2017 Dynamics of hybrid mechanical-electromechanical locally resonant piezoelectric metastructures *ASME. Smart Materials, Adaptive Structures and Intelligent Systems, Volume 2: Modeling, Simulation and Control of Adaptive Systems; Integrated System Design and Implementation; Structural Health Monitoring* V002T03A035 (<https://doi.org/10.1115/SMASIS2017-3948>)
- [81] Wang G, Cheng J, Chen J and He Y 2017 Multi-resonant piezoelectric shunting induced by digital controllers for subwavelength elastic wave attenuation in smart metamaterial *Smart Mater. Struct.* **26** 25031
- [82] Kurdila A J and Tarazaga P 2018 *Vibrations of Linear Piezostructures* (New York: Wiley)
- [83] de Marneffe B and Preumont A 2008 Vibration damping with negative capacitance shunts: theory and experiment *Smart Mater. Struct.* **17** 35015
- [84] Paruchuri S T, Kurdila A J, Sterling J, Vignola A, Judge J, Vignola J and Ryan T 2017 Thermodynamic variational formulations of subordinate oscillator arrays (SOA) with linear piezoelectrics *ASME. Int. Design Engineering Technical Conf. and Computers and Information in Engineering Conf., 29th Conf. on Mechanical Vibration and Noise* V008T12A068 (<https://doi.org/10.1115/DETC2017-68056>)
- [85] Paruchuri S T, Sterling J, Kurdila A and Vignola J 2017 Piezoelectric composite subordinate oscillator arrays and frequency response shaping for passive vibration attenuation *2017 IEEE Conf. on Control Technology and Applications (CCTA) (Mauna Lani, HI, 2017)* pp 702–7
- [86] Preumont A 2006 *Mechatronics: Dynamics of Electromechanical and Piezoelectric Systems* (Dordrecht: Springer)
- [87] Yu Y-Y 1996 *Vibrations of Elastic Plates* (New York: Springer)
- [88] Yang J 2005 *An Introduction to the Theory of Piezoelectricity (of Advances in Mechanics and Mathematics vol 9)* (Boston, MA: Springer)
- [89] Leo D J L 2007 *Engineering Analysis of Smart Material Systems* (New York: Wiley)
- [90] Karnopp D C, Margolis D L and Rosenberg R C 2012 *System Dynamics: Modeling, Simulation, and Control of Mechatronic Systems* (Hoboken, NJ: Wiley) 978-0-470-88908-4
- [91] Erturk A and Inman D J 2011 *Piezoelectric Energy Harvesting* (Chichester: Wiley)
- [92] Meirovitch L 1970 *Methods of Analytical Dynamics* (New York: McGraw-Hill)